UNIVERSIDAD EAFIT

Engineering School

Design Engineering Research Group (GRID)

Viability of vertical building integrated photovoltaics in tropical regions: an experimental approach

Graduation manuscript presented as partial requirement to obtain the

Master in Engineering

(Draft Document: Version 11/03/2021)

AUTHOR:

Ing. Juan Pablo Giraldo Pérez

ADVISOR:

MSc. Alejandro Velásquez López

January 2021

Abstract

Solar energy is expected to be the fastest developing of the Renewable Energy Sources (RES) in the next years. With the introduction of Distributed Generation (DG) into space limited urban areas, the need to find new solutions that allow the installation of Photovoltaic (PV) systems in the cities has become crucial for the constant and sustainable energetic development of the world. This study presents experimental analyses of the implementation of vertical Building Integrated Photovoltaics (BIPV), one of the most accepted alternatives for the installation of PV technologies in urban areas. Emphasis is made on finding the viability of such technologies in tropical regions from an energy generation standpoint. The influence of irradiance, humidity and air temperature on power generation was also evaluated in order to identify how these meteorological conditions affect the performance of BIPV on these regions of the globe. The results suggest that the implementation of these technologies is viable for urban spaces in the studied regions as it was found that east and west facing vertical modules require only twice the space of horizontal ones to equal their energy generation. Urban areas' buildings count with up to 20 times larger vertical available areas in comparison to the horizontal ones, meaning that overall these have a higher energy generation potential. It was also found that while humidity and temperature had a small impact on the power generation of the BIPV modules, irradiance had a strong linear correlation with it.

Keywords: Solar Energy, Building Integrated Photovoltaics, Renewable energy sources.

Resumen

Se espera que la energía solar sea la fuente de energía renovable de más rápido desarrollo en los próximos años. Con la introducción de los sistemas de generación distribuida en áreas urbanas con espacios limitados, la necesidad de encontrar nuevas soluciones que permitan la instalación de sistemas fotovoltaicos en las ciudades se ha vuelto crucial para el desarrollo energético constante y sostenible del mundo. Este estudio presenta análisis experimentales de la implementación de sistemas de tipo "Building Integrated Photovoltaics (BIPV)" verticales, una de las alternativas más aceptadas para la instalación de tecnologías fotovoltaicas en áreas urbanas. Se hace énfasis en comprobar la viabilidad de tales tecnologías en las regiones tropicales desde el punto de vista de la generación de energía. También se evaluó la influencia de la irradiancia, la humedad y la temperatura del aire en la generación de energía para identificar cómo estas condiciones meteorológicas afectan el desempeño de estas tecnologías cuando son usadas en estas regiones del mundo. Los resultados sugieren que la implementación de estas tecnologías es viable para los espacios urbanos en las regiones estudiadas, ya que se encontró que los módulos verticales orientados al este y al oeste requieren solo el doble de espacio que los horizontales para igualar su generación de energía, adicionalmente las áreas verticales disponibles en edificios pueden ser hasta 20 veces más grandes que las horizontales, lo que significa que cuentan con un mayor potencial de generación de energía. También se encontró que mientras la humedad y la temperatura tuvieron un menor impacto en la generación de energía de los módulos de tipo BIPV, la irradiancia presentó una fuerte correlación lineal con esta.

Palabras Clave: Energía Solar, "Building Integrated Photovoltaics", Fuentes de Energía Renovable.

Personal publications

Several scientific contributions were generated and published during the development process of this research project:

Conferences:

- Giraldo-Pérez, J. P., Orrego-García, J. S., Ospina-Metaute, C. C., and Velásquez-López, A. (2020). "Simplified method to compare the performance of a solar cell under different optical conditions and orientations". In Figueroa-García, J. C., Garay-Rairán, F. S., Hernández-Pérez, G. J., and Díaz-Gutierrez, Y., editors, *Applied Computer Sciences in Engineering*, pages 477-488, Cham. Springer International Publishing. ISBN: 978-3-030-61834-6. DOI: 10.1007/978-3-030-61834-6_41.

Journal:

- Juan Pablo Giraldo-Pérez , Juan Sebastian Orrego-García, Cristian C. Ospina-Metaute, Alejandro Velásquez-López and Esteban Betancur "Performance and viability of vertical BIPV in tropical zones: an experimental and simulation approach." To be submitted to *Solar Energy*, Elsevier. ISSN: 0038-092X. Indexed in Scopus (Q1) and Clarivate (Q2).

Acknowledgements

Firstly I would like to thank my family and friends for their continuous support during all the stages of this master project. Secondly I would like to thank my advisor Alejandro Velásquez López for giving me the opportunity to work on this project alongside him. To all the members of the GRID who had a direct and indirect impact in my work, thank you for your time and effort to create a space in which we could improve our research experience though the socialization of questions, research process and results, which I believe was one of the most important factors for the success to this project.

I would like to also thank Universidad EAFIT and the alliance "ENERGETICA 2030", which is a Research Program, with code 58667 from the "*Colombia Científica*" initiative, funded by The World Bank through the call "778-2017 Scientific Ecosystems". The research program is managed by the Colombian Ministry of Science, Technology and Innovation (Minciencias) with contract No. FP44842-210-2018.

Contents

List of Figures

List of Tables

Chapter 1

Introduction

1.1 Background

Energy is a fundamental element for the proper social, economical and technological development of the world (Owusu and Asumadu-Sarkodie, 2016). Historically fossil fuels (Oil, Coal and Natural Gas) have been our main sources of energy, powering transportation, industries and the generation of electricity. However, the way energy is produced will dramatically change over the next decades. The awareness of climate change and sustainability will turn the world away from fossil fuels towards cleaner and renewable energy sources (Owusu and Asumadu-Sarkodie, 2016).

By 2050, electricity is expected to become our main energy source, with a share of 40% of the global energy demand (DNVGL, 2017a). As electricity demand grows, Non-Conventional Renewable Energy Sources (NCRES) will become the primary agent of our power generation scheme. Figure 1.1 shows the forecast of electricity generation by source for the year 2050, indicating that 72.2% of the global production is expected to come from solar and wind power (DNVGL, 2017). Solar energy is the fastest growing clean energy generation technology and is predicted to supplying as much as 35.8% of the global electricity demand by 2050 (DNVGL, 2017b).

In a Latin American context, and more specifically in Colombia, by 2020 there was an installed electricity generation capacity of 16.8GW, out of which just 0.03GW accounted for NCRES. Given its geological conditions, the country has mainly taken advantage of its fresh water sources to generate hydroelectric power, which covers 68.3% of the country's electricity demand (Acolgen, 2020). This extended use of hydroelectric resource makes Colombia one of the cleanest countries when it comes to average grams of CO_2 per kWh generated with 164.38 g/kWh(XM, 2020a), well below the world average of 340 g/kWh (IEA, 2019). However, although hydroelectric power is considered to be a renewable energy source, it does have impacts on the environment such as changes on the water chemistry, sedimentation, flow regime and the fact that it directly affects the living organisms which

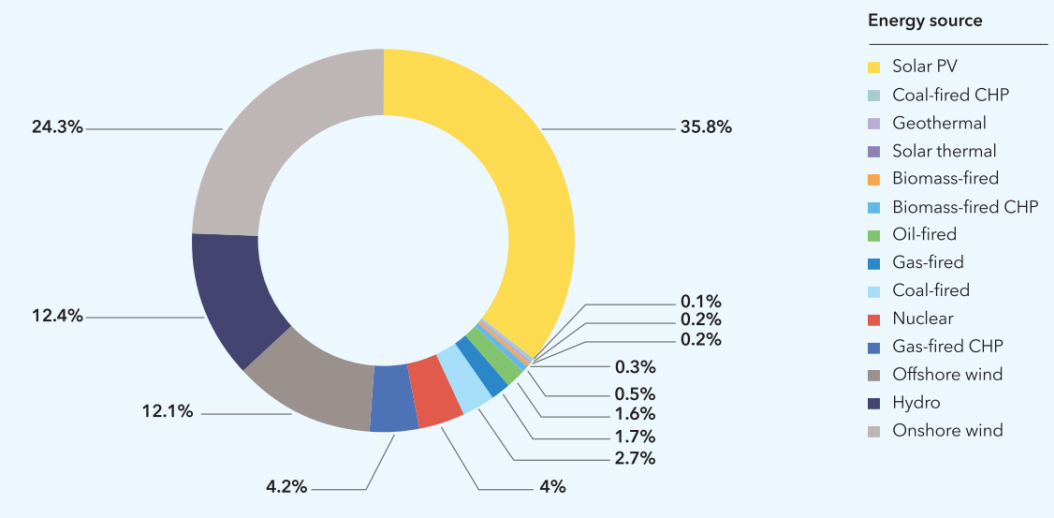

Figure 1.1: Forecast of the world electricity generation for the year 2050 (DNVGL, 2017)

interact with the water sources (McCartney, 2009).

Given the path the world has taken towards the implementation of NCRES, in 2014 the Colombian congress passed the law 1715 with the goal of promoting the development and use of these technologies in the country. As a result, according to XM, Colombian company in charge of the real-time monitoring and management of the country's interconnected electricity network, it is expected that by the year 2023 over 2GW of new solar and wind power plants will be built and connected to the network (XM, 2020b; EnergíaEstratégica, 2020).

In addition to this, the country is also preparing for a big transformation in the way energy is generated, stored, transmitted and used. As presented in the document "Smart Grids Colombia Visión 2030" by the "Unidad de Planeación Minero Energética" (UPME) (BID, 2016), Colombia is already setting the bases for the implementation of Smart Grids, a concept that involves more intelligent electricity networks which enable not only the flow of electricity, but also of real time information of how the energy is being used and generated. One of the main changes proposed by these new networks is the Distributed Generation (DG), a new power generation scheme which introduces the implementation of smaller and modular energy generation devices, these new devices would be located close to the consumers and use Renewable Energy Sources (RES) (e.g. solar photovoltaic, wind and biomass) as their main power source (Allan et al., 2015).

For developing countries such as Colombia, DG represents an opportunity not only to reduce greenhouse emissions, but also bring electricity to remote rural areas that are currently uncovered by the National Interconnected Electricity Network or that have instability issues with their electricity supply, potentially improving the life conditions of the population in such areas (Rodríguez-Urrego and Rodríguez-Urrego, 2018; Shahsavari and Akbari, 2018). However, the implementation of DG in

cities and their densely populated areas represent a challenge due to the lack of available space. In the case of Photovoltaic (PV) technologies, traditional systems are calculated, designed and optimized to receive the maximum possible irradiation (Gharakhani Siraki and Pillay, 2012; Laveyne et al., 2020) and thus generally require large areas for their optimum functioning.

Given the world's main cities' characteristic of rapid growth in numbers of buildings with considerable height (Ali and Al-Kodmany, 2012), new developments such as Building Integrated Photovoltaics (BIPV) are now opening the possibility of making use of these building's surfaces (e.g. facades and roofs) for the installation of photovoltaic systems (Jelle, 2016), overcoming the lack of space. Particularly, facades applications represent 20% of the BIPV market (Shukla et al., 2017) with a growth trend given the further reduction of available horizontal areas for traditional PV installations.

1.2 Research Problem Definition

Even though BIPV represents an opportunity to implement DG in cities, it is important to remember that its performance will be less in comparison with the traditional PV systems. This is even more critical in the case of installations on facades as vertical orientations are not optimal for PV modules (Díez-Mediavilla et al., 2019). For this reason research is needed to identify the factors that would allow performance optimization of these technologies and to evaluate if its implementation is viable.

Previous studies regarding the use of vertical BIPV technologies in buildings' facades have taken two different approaches to calculate the performance of such systems. On the one hand, modern software and models have been used to study and estimate the energy generation capabilities of these systems taking into consideration the building's morphology (Ospina-Metaute et al., 2020) and the urban structure where it is located (Jakubiec and Reinhart, 2013; Brito et al., 2017; Redweik et al., 2013; Hsieh et al., 2013; Jaugsch and Löwner, 2016). On the other hand, experimental approaches have been implemented in which solar panels or pyranometers are used to determine the amount of energy that can be generated by these surfaces and how it is affected by its surroundings (Díez-Mediavilla et al., 2019; Revesz et al., 2018a).

Although these studies come to the same conclusion that vertical systems receive less solar radiation than horizontals ones, they also found that when combining the solar irradiation reaching two or more facades of a building, it can not only be equal but excel the amount that is reaching the horizontal surface of the roof (Kumar et al., 2018). In addition, facades have larger surface areas which, in high-rise buildings, can get up to 20 times larger than roof areas (Pérez et al., 2014). This means there is more available solar energy on the facades, even though the roofs get higher levels of irradiation.

Literature found and presented in this section, which is further expanded and explained in chapter 2, shows that the northern temperate climatic zone (latitudes 23.5°N to 66.5°N) has been the most

explored in the behavior of BIPV technologies (Biyik et al., 2017). Specifically, Europe is the region in which the majority of the studies, both experimental and simulated, have taken place. For this reason the information available is only accurate for these geographical locations as it is well known that the performance of PV technologies is dependent not only on orientation but on climatological and geographical conditions (Biyik et al., 2017; Kumar et al., 2020). The literature review did not show any evidence of previous experimental research made in tropical regions (latitudes 23.5°S to 23.5°N) in relation to BIPV from the perspective of comparing horizontal and vertical generation. However, these regions possess a high potential for the implementation of PV technologies thanks to its climatological and geographical conditions (Vargas Gil et al., 2020). Equatorial countries like Colombia, for example, present the advantage of having high levels of irradiation that remains constant throughout the year (Soonmin et al., 2019; Carvajal-Romo et al., 2019).

The purpose of this study was, therefore, to explore the performance and viability of the implementation of vertical BIPV in tropical regions, comparing it against the traditional horizontal modules and to explore how the climatic variables of such regions affect their electricity generation.

1.3 Research question

The following question was established as the core of this research.

How does the performance of vertical BIPV compare to horizontal ones when installed in tropical regions and how are the meteorological variables related to the their power generation?

1.4 Objectives

In order to answer the research question, one general objective and three specific objectives were proposed to guide this research, giving clear goals and milestones to the course of the same.

1.4.1 General objective

To identify the differences between the performance of vertical and horizontal BIPV located in tropical regions and how their energy generation relates to the meteorological variables, through the implementation of field tests for the acquisition of data and analysis of solar cells' electrical variables, in order to evaluate the energetic viability of the implementation of vertical BIPV in these regions.

1.4.2 Specific objectives

- Identify the main properties of solar cells, how their performance is evaluated and how previous studies approached vertical BIPV through search and analysis of academic and commercial

literature to acquire the necessary knowledge and tools to appropriately direct the research.

- Collect data through the design and implementation of a device and monitoring system capable of simultaneously measuring multiple solar cells' performance.
- Make statistical analyses of the acquired data to elaborate conclusions on the performance of BIPV at each location and orientation used.

1.5 Research justification

This section will describe the theoretical and social relevance of this project.

As previously stated, no literature was found to have taken an experimental approach to evaluate and discuss the performance of vertical BIPV in tropical regions. This document and all the additional publications written around this project (e.g. conferences and journal articles) will reduce this knowledge gap and present further information on this topic that is of great interest due to the expected expansion of PV technologies and DG over the next years. In addition to this, and as explained in section 1.1, the results of this study could play an essential roll in improving the life quality to communities that currently have no access to electricity.

The interaction with the research community and reporting of the results is crucial for the continuous development of this topic as it could guide other authors into identifying new research areas and gain interest in topics such as:

- Influence of climatic variables on BIPV technologies.
- Implementation of vertical BIPV in tropical regions.
- New technologies for the implementation of PV systems in urban areas.
- DG and its application in urban areas of tropical regions.
- Differences between the implementation of PV technologies in different climatic zones.

Finally, this project directly aligns with two of the Sustainable Development Goals (SDGs) proposed by the United Nations in 2015. SDGs number 7 (afordable and clean energy) and 11 (sustainable cities and communities).

1.6 Research Scope

The scope of this project is defined by the following points:

- The electrical variables to be measured and analyzed from the solar modules are the Open-Circuit Voltage (Voc) and Short-Circuit Current (Isc), which will be used to get an estimate of their power generation. For further information on this method refer to chapter 3.

- The climatic variables to be used in the analysis will be taken from the meteorological stations of the alliance "Energética 2030" of which this research is part of.
- The locations used as representatives for the tropical regions are the cities of Llanogrande and Envigado, both located in Colombia. For further information on the selection of these locations refer to section 3.4.
- The vertical orientations to be evaluated are East and West.
- The tests will be performed on monocrystalline solar cells of reference C60 and manufactured by the company SunPower. For further information on the modules and their selection refer to section 3.

1.7 Research Approach

The present study was carried out following the methodology Design Inclusive Research. As described by Horváth (Horváth et al., 2007), this approach allows the inclusion of design in the research process. For the case of this study, and as expressed in the second specific objective, the design of a measuring hardware is used as part of the research process.

The methodology consists of three phases, each one corresponding to each of the specific objectives presented in section 1.4.2. Phase one consists of exploratory research actions, phase two is creative design and phase three is the confirmative research actions. Figure 1.2 pictures how is the interaction between the methodology and the presented specific objectives.

1.8 Thesis organization

The manuscript structure is as follows, Chapter 2 synthesizes the state of the art and literature review that was relevant for the development of the study. The information in this chapter helps to understand the basis of PV technology, how it works, how its performance is evaluated, what affects its performance and how it is being integrated into buildings in the form of BIPV. Chapter 3 presents the design and development of the proposed solar cell measuring hardware and experiments. The design process explained in this chapter includes working principle, tests, redesigns and final product. Lastly, it presents the information of the experiments that were proposed and carried out to answer the research questions. Chapter 4 presents the results of the experiments. The differences between horizontal and vertical modules and the correlation between electrical and climatic variables is discussed. Finally chapter 5 presents the conclusions of the study, answers to the research questions and discusses possible future research pathways.

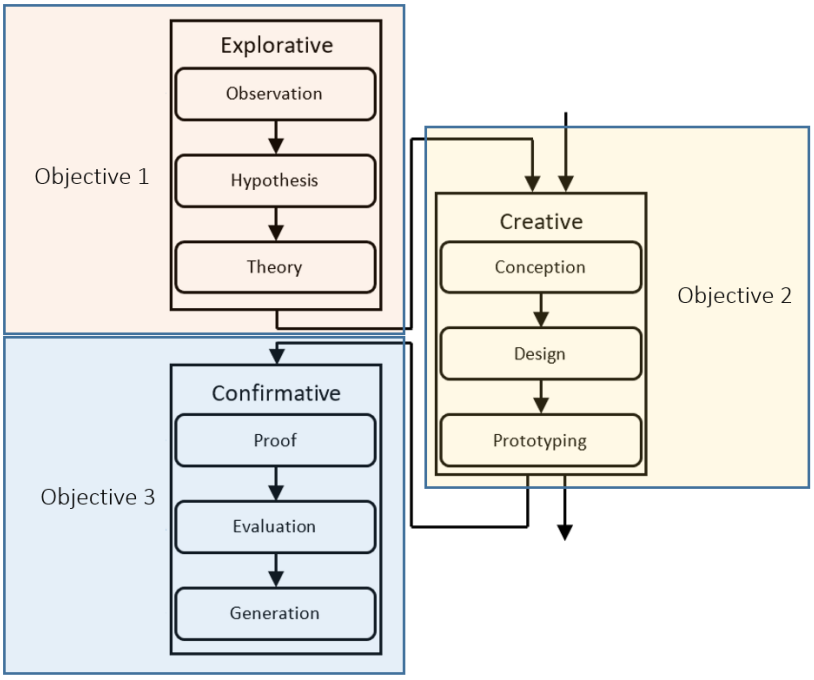

Figure 1.2: Design Inclusive Research methodology (Horváth, 2008)

Chapter 2

State of the Art

This chapter presents the basic concepts related to solar cells, different methods used to evaluate their performance and the factors that affect its energy generation.

2.1 Photovoltaic Cells

A PV Solar Cell is an electronic device that converts solar energy (irradiation) into electric energy, generating power without moving parts nor directly producing pollution. This energy transformation works by the "photovoltaic effect", a process carried out by materials capable of creating electron-holes (separation of electrons from their orbits) when excited by high energy photons. This excited free electrons are then conducted to an external circuit and back into to the PV material, generating a current through the circuit (C.B.Honsberg, 2019).

There are remarkable developments on PV materials and manufacturing methods, each with specific mechanisms to improve light conversion into electrical energy. Nowadays, semiconductor materials in the form of a p-n junction such as silicon dominate the market (Singh, 2009; Zhang et al., 2014), reaching power conversion efficiencies of up to 29.1% in research labs (NREL, 2019a) and 24.4% in commercial modules (NREL, 2019b).

2.2 IV Curve

An ideal solar cell can be represented as a current source in parallel with a diode as shown Figure 2.1. Therefore, its current and voltage characteristics are described by Shockley's diode equations (equations 2.1 and 2.2), where I_{ph} is the photo-generated current, I_0 is the diode dark saturation current, n is the ideality factor, T is the temperature and K_0 is Boltzmann constant. For the mathematical analysis of a real (non-ideal) solar cell, these equations should be complemented with the shunt and

series resistances which reduce the efficiency of the solar cell by dissipating power (Kalogirou, 2017).

$$I = I_{ph} - I_0 \left[e^{\frac{qV}{nkT}} \right] \tag{2.1}$$

$$V = \frac{nkT}{q} \ln \left(\frac{I_{ph} - I_0}{I} \right) \tag{2.2}$$

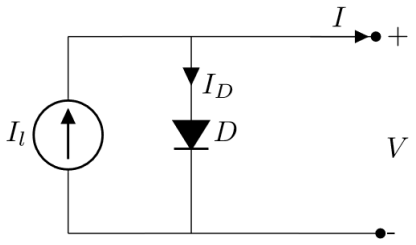

Figure 2.1: PV Cell Model.

The equations above can be plotted as an I-V curve as shown in Figure 2.2. This curve is unique to every PV solar cell reference and presents some of their fundamental characteristics.

- **Maximum Power Point (MPP):** Point at which the cell achieves its maximum efficiency. The points V_{MPP} and I_{MPP} correspond to the voltage and current generated by the cell at the MPP.
- **The Short-Circuit Current (Isc):** It is the maximum current generated by the solar cell, it occurs when the voltage across its terminals is zero. Its value depends on the area of the solar cell, number of photons reaching it, spectrum of the incident light and its optical properties such as absorption and reflection.
- **The Open-Circuit Voltage (Voc):** It is the maximum voltage achievable by the solar cell, it occurs when the net current though the device is zero.
- **The Fill Factor (FF):** This property is an important determiner of a solar cell efficiency. It is defined as the ratio of the maximum power of the solar cell (MPP) to the product of Open-Circuit Voltage (Voc) and Short-Circuit Current (Isc), as shown by equation 2.3. Graphically, the FF is a measure of the "squareness" of the solar cell I-V Curve, in Figure 2.2 it would be equal to the ratio between rectangles A and B.

$$FF = \frac{V_{MPP} I_{MPP}}{V_{OC} I_{SC}} = \frac{P_{MPP}}{V_{OC} I_{SC}} \tag{2.3}$$

- **The efficiency:** It is defined as the ratio of energy generated by the solar cell to the input energy (irradiance) as presented by equation 2.4. It depends on the spectrum and intensity of

the incident sunlight, the temperature of the solar cell and other electrical and climatological variables.

$$\eta = \frac{P_{MPP}}{P_{in}} = \frac{V_{OC} I_{SC} FF}{P_{in}} \tag{2.4}$$

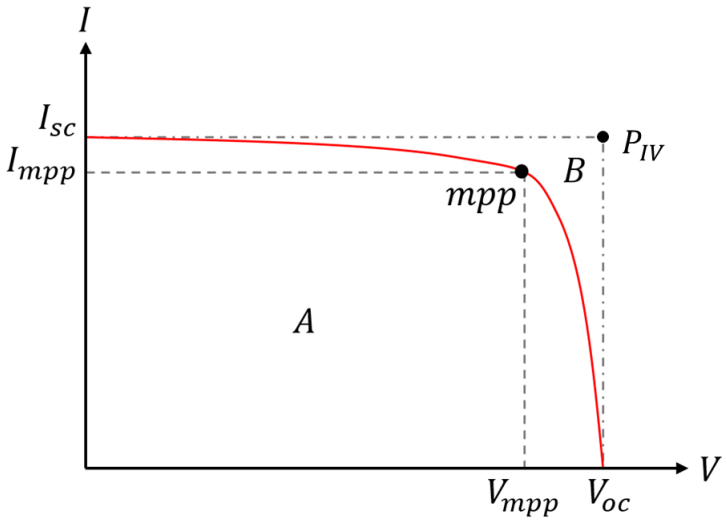

Figure 2.2: IV curve of a solar cell.

2.3 IV Curve Tracers

Given the interest from both industrial and academic groups for maximizing the efficiency of solar cells, the usage of instruments that allow precise measurements of their energy generation and response to external variables becomes an important asset for future developments. IV curve tracers are generally the to-go solution for this kind of analyses as these are capable of giving critical information like Open-Circuit Voltage (Voc), Short-Circuit Current (Isc), P_{mpp}, I_{mpp}, V_{mpp}, Fill Factor (FF), among others. However, multiple research-grade instruments have been found on academic literature for the evaluation of more precise or specialized technologies and experiments, for example, the characterization of elements that operate under the nano-ampere scale (Luna et al., 2014), characterization and status check of photovoltaic systems in partial shade conditions (Ramaprabha et al., 2015) or the implementation of virtual tools for online monitoring of photovoltaic systems (Riley and Tolbert, 2015).

2.3.1 IV Curve Tracer Topology

Curve tracers use multiple methods to acquire data, the key differences between methodologies are given by variables such as precision, sweep speed, measuring range and resolution.

2.3.1.1 Resistive Load

This method is the easiest way to obtain the IV curve of a photovoltaic system, it consists on connecting a variable resistance to the terminals of the solar module and varying it from 0 ohms to "infinite" while keeping track of the values obtained for the voltage and the current starting from the Isc (0 resistance) and finalizing on the Voc (infinite resistance). The variation of the resistance can be done manually (Mahmoud, 2006), but this process is slow, the irradiation can vary and the thermal conditions of both the environment and the cell might change, making the measurements highly imprecise. Another way to apply this method is by implementing an algorithm that allows varying the resistance and measuring voltage and current in short intervals of time (Willoughby et al., 2014). Figure 2.3 show a schematic of this method.

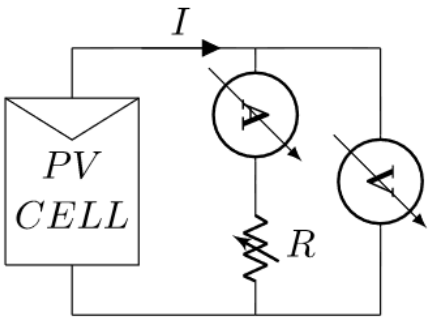

Figure 2.3: Variable resistance schematic (Durán et al., 2008).

One of the main disadvantages of this approach is that when the resistance is increased linearly the slope of the measured points acts like a tangent function, which causes a densification on the measured data points as it comes closer to the maximum value of the resistance (Voc), creating a measurement-free section on the IV curve as seen in Figure 2.4, limiting the range of possible measurements, for this reason the results obtained by this method should be treated as an approximation (Durán et al., 2008).

An alternative version of this method consists in a combined system of resistances and computer-controlled switches which open and close to vary the resistance from 0 to a desired maximum value by combining multiple resistances in series (Rivai and Rahim, 2014). With this configuration complete measuring cycles with times as low as 540ms were achieved. The schematic of the proposed system is shown in Figure 2.5.

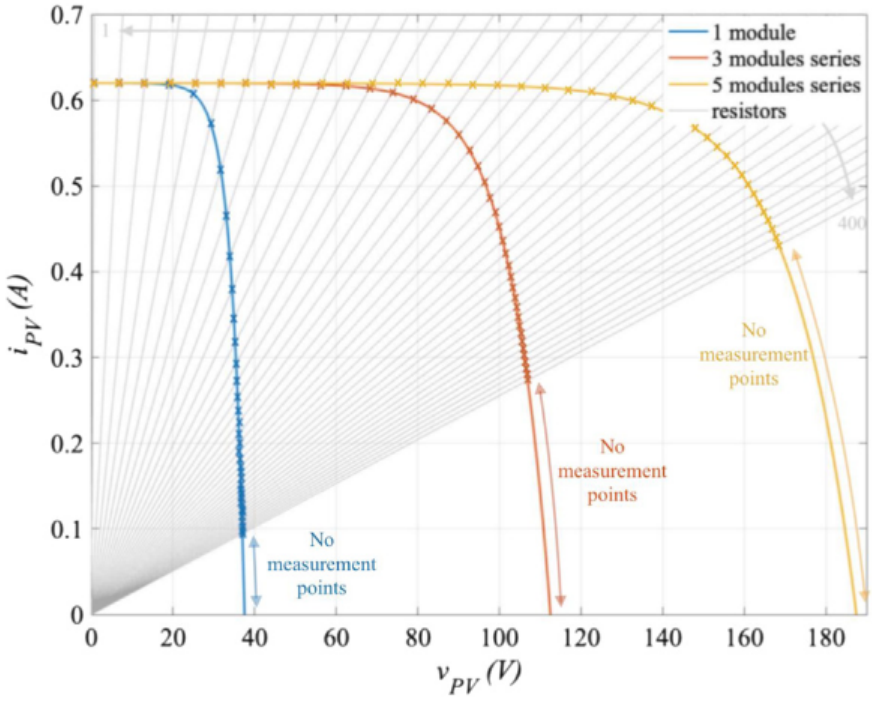

Figure 2.4: IV curve generated by the resistive load method (Zhu and Xiao, 2020).

2.3.1.2 Capacitive Load

This method proposes the usage of capacitors to obtain the IV curve. Due to the electrical behavior of capacitors, as they charge, the current decreases and the voltage increases, which allows the curve to be obtained in a passive way (Erkaya et al., 2014). The voltage and the current are measured on the terminals of the solar cell as shown in Figure 2.6. A resistance is used as a load to discharge the capacitor once the test is finished. This method is capable of obtaining the curves in short periods of time, however, the required capacitance highly depends on the characteristics of the photovoltaic technology being tested, specially the voltage that the system is able to produce. The red zone shown in Figure 2.7 presents the relation of voltage and capacitance needed to properly make the curve evaluation.

The selection of the required capacitance value is given by equation (2.5), where C_{load} is the value of the capacitance, N_p is the number of parallels, N_s is the number of solar modules in series, and t_{charge} is the load time of the capacitor. It is recommended that this time is established in a range between 20 ms and 100 ms (Reischauer and Rix, 2019).

$$C_{load} = 0.55 \frac{t_{charge} I_{sc} N_p}{V_{oc} N_s} \tag{2.5}$$

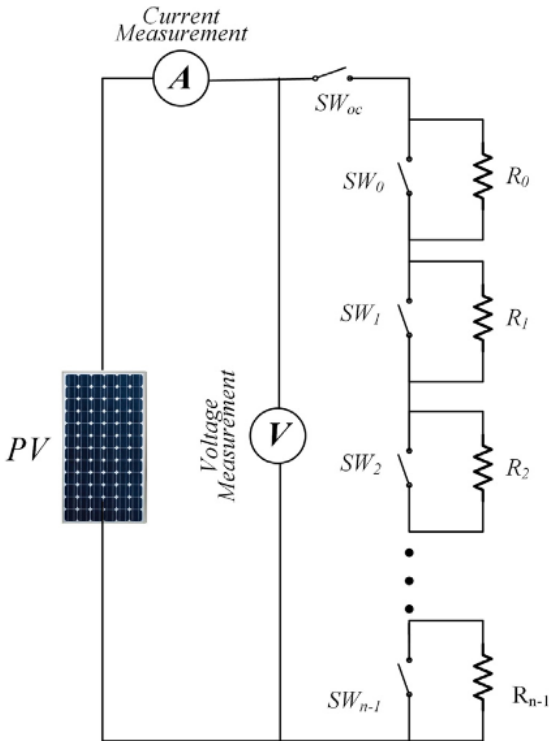

Figure 2.5: Resistive load schematic (Rivai and Rahim, 2014).

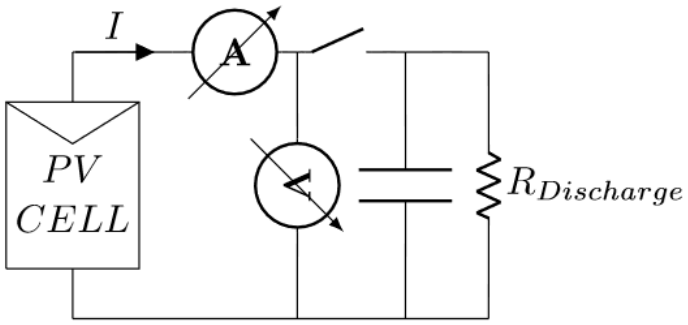

Figure 2.6: Capacitive load schematic (Zhu and Xiao, 2020).

2.3.1.3 Electronic Load

This method usually uses a transistor as an electronic load, being the BJT (Bipolar Junction Transistor), IGBT (Insulated Gate Bipolar Transistor) and MOSFET (Metal oxide Semiconductor Field Effect Transistor) the most common ones. By making use of the transistor's operating regions (cut, lineal and saturation) precise measurements of voltage and current can be obtained in short periods of time (Guerriero et al., 2018). When an increasing voltage, starting at $0V$, is applied to the gate terminal of the transistor (in the case of a MOSFET), it allows a current flow through the circuit

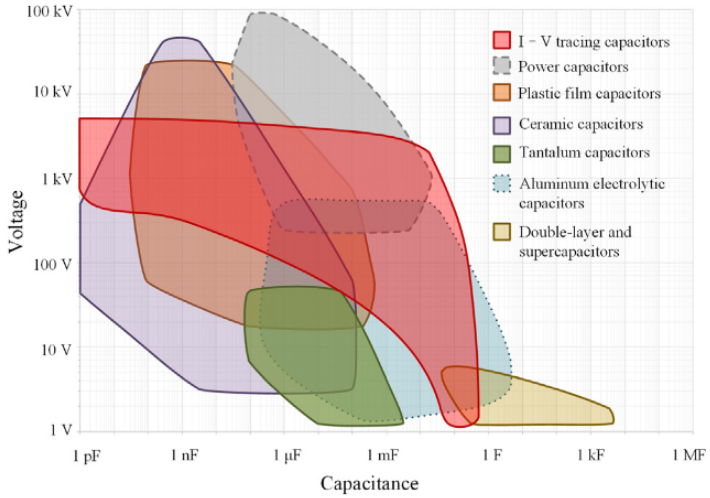

Figure 2.7: Capacitance required according to the voltage of the photovoltaic array (Zhu and Xiao, 2020).

starting at $0A$ and increasing until Isc while simultaneously decreasing the voltage from Voc to $0V$. This procedure can be done in a scale of ms, reducing the effects of the thermal and climatological related fluctuations on the data obtained (Willoughby and Osinowo, 2018). Figure 2.8 shows a scheme for this method applied using a MOSFET.

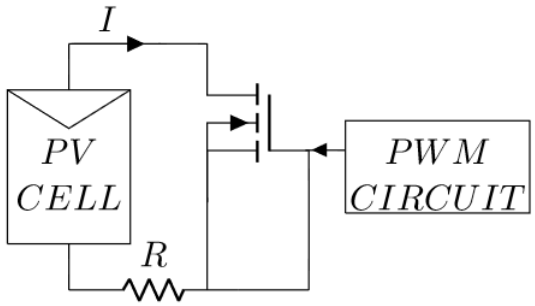

Figure 2.8: MOSFET as electronic load (Willoughby and Osinowo, 2018).

2.3.1.4 Four-quadrant Power Supply

This method consists on using a Four-quadrant Power Supply, a device that can be used as a source or as a sink for currents with bipolar voltage (positive or negative voltage). The IV curve of photovoltaic systems is characterized using the first quadrant, which corresponds to the power supply as a sink (Figure 2.9), however, quadrants 2 and 4 can be used in other test and diagnoses of the solar cells (Hecktheuer et al., 2002).

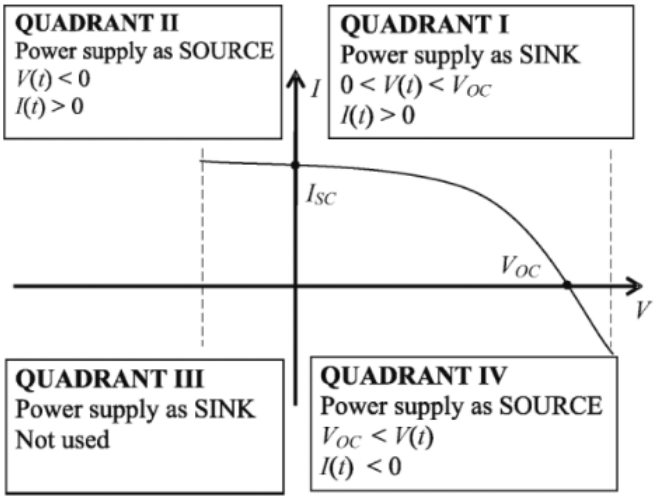

Figure 2.9: Working quadrants (Piliougine et al., 2011).

The Power Supply is controlled by a computer and connected directly to the solar module as showed in Figure 2.10. The computer is programmed to do a voltage sweep on a defined range while saving the voltage and current measurements. These devices can work with maximum voltage and current values of 1000V and 100A, however, this method is currently restricted to be used only in laboratories as it is more complex and requires specialized equipment.

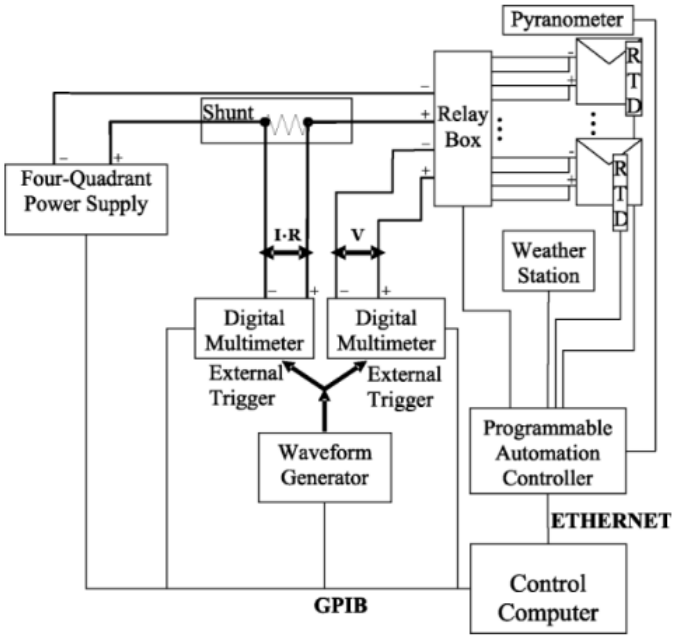

Figure 2.10: Four-quadrant Power Supply schematic (Piliougine et al., 2011).

2.3.1.5 DC-DC Converter

This method uses DC-DC converters in order to emulate virtual resistance loads on the photovoltaic module terminals and generate the IV curve. The converters can measure in two regimes, the first one is the Continuous Conduction Mode (CCM) and the second one is the Discontinuous Conduction Mode (DCM) (Durán et al., 2012). The mode of operation is given by the dimensionless parameter K, which is given by the expression (2.6)

$$K = \frac{2L_{eq}f_s}{R} \tag{2.6}$$

Being L_{eq} the equivalent inductance and R the resistive load. When K is higher than K_{crit} value a CCM operation will take place and otherwise a DCM operation will take place. K_{crit} value varies according to the topology of the DC-DC Converter used, Figure 2.11 shows the most common ones.

Table 2.1 shows the relation between R, working cycle D and the resistive load emulated R_i.

	Buck Converter	**Boost Converter**	**Buck-Boost Derived Converter**
R_i (CCM)	$\frac{R}{D^2}$	$R(1-D)^2$	$\frac{R(1-D)^2}{D^2}$
R_i (DCM)	$\frac{R}{4}\left(1+\sqrt{1+\frac{4K}{D^2}}\right)^2$	$\frac{4R}{\left(1+\sqrt{1+\frac{4K}{D^2}}\right)^2}$	$\frac{KR}{D^2}$
K_{crit}	$1-D$	$D(1-D)^2$	$(1-D)^2$

Table 2.1: Relationship between R_i, R, D (Duran et al., 2008).

2.3.2 Commercial IV Curve Tracer

There are several commercial devices designed to characterize the solar cells' electrical variables and IV curves. Table 2.2 presents examples of different models, prices and technical details for some commercial I-V curve tracers.

PV Analyzer Model	**Price (US$)**	**Specifications**					
		PV Voltage Range (V)	**Voltage Resolution (mV)**	**Current Resolution (mA)**	**I-V Trace Points**	**Company**	**Sweep Time (s)**
SOLAR-600	3,000	0-60	10	10	-	Amprobe	3
PVA-1500V2	9,895	0-1500	25	2	100-500	Solmetric	0.05-2
PV210	2,595	0-1000	100	10	-	Seaward	-
I-V500W	4,495	0-1500	100	10	-	HT-Instruments	5
FTV200	4,129	0-1000	100	10	500	Chauvin-Arnoux	-

Table 2.2: I-V Curve tracers (Amprobe, 2010; Corporation, 2018; Electronic, 2018; Instruments, 2019; Arnoux, 2012).

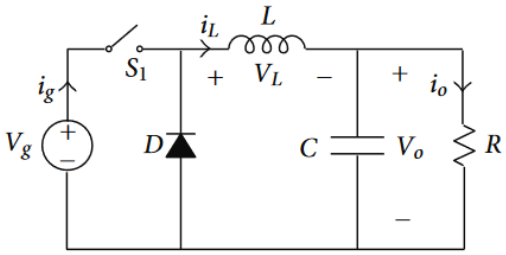

(a) Buck Converter.

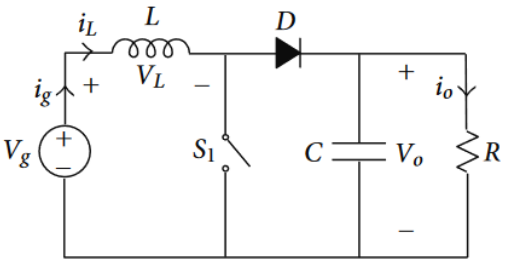

(b) Boost Converter.

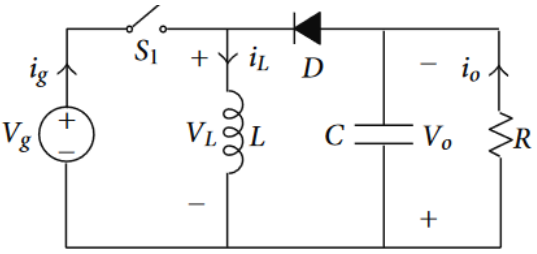

(c) Buck-Boost Converter.

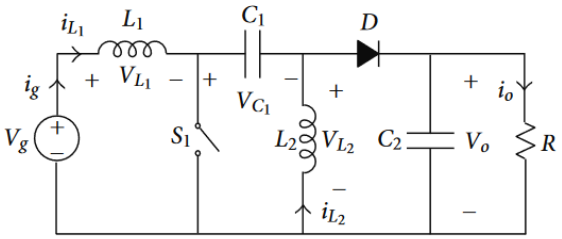

(d) Sepic Converter.

Figure 2.11: Topologies for DC-DC Converter (Durán et al., 2012).

These IV curve tracers use some of the previously discussed methods as capacitive load and DC-DC Converter to get their measurements (Durán et al., 2008; Zhu and Xiao, 2020). The difference between these methods are, as previously mentioned, accuracy, sweep speed, maximum rating and resolution. However, the downside of these devices and methods include complexity, price and the fact that they are designed to evaluate one solar cell or module at a time. When multiple cells need to be assessed simultaneously, for instance to compare their performance with different optical arrangements or orientations, it is necessary to have as many measuring instruments as cells being compared, which is not cost-effective nor easy to implement. In addition, these measurement instruments are not stand-alone, meaning that they require the presence and manipulation of a user to start, operate, retrieve and save data.

2.4 Factors that affect the efficiency of solar cells

The efficiency of solar cells can vary as they are subjected to various factors which can go from environmental to manufacturing and installation variables. This section will discuss some of the most relevant climatic variables that have a direct impact on the energy generation of PV cells.

2.4.1 Irradiance

Irradiance is the most directly related variable to play a role in the energy produced by solar cells since, as discussed in section 2.1, the physical phenomenon by which the cells work purely depends in the intensity of irradiance and energy of its photons (C.B.Honsberg, 2019). The intensity of the irradiation mainly depends on two factors, the weather and the sun's location in the sky (Mondol et al., 2007). Moreover, irradiation can be separated in three categories: direct, diffuse and reflected irradiation.

Irradiation and energy output of solar cells have a directly proportional relationship, meaning that whenever the irradiation increases, the generation of energy will also increase, and the same behaviour occurs in case of decreasing irradiation (Shahatha Salim et al., 2013). Figure 2.12 presents the results of a study carried out on this topic, the graph shows the IV curve of a solar cell under different intensities of irradiation Yau et al. (2013).

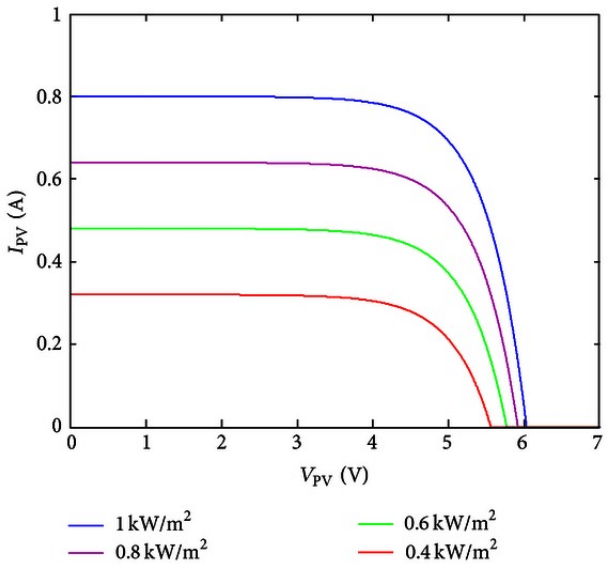

Figure 2.12: Effect of irradiance on solar cell's behaviour (Yau et al., 2013).

2.4.2 Temperature

Changes in the environmental temperature where the cell is located also have an effect over its efficiency. Overheating caused by the combination of high irradiance and high ambient temperatures can highly affect the performance of the cell. The temperature of the module T_m can be described as a function of the environmental temperature T_{amb}, the incident irradiation E and the Normal Operating Cell Temperature $NOCT$, as described by the equation (2.7).

$$T_m = T_{amb} + \frac{(NOCT - 20)E}{800} \tag{2.7}$$

The temperature of the cell and the Voc have an inversely proportional relationship, this means that whenever temperature goes up, the voltage decreases (Moharram et al., 2013) as shown in Figure 2.13. For the specific case of mono and polycrystalline cells, the voltage decreases around 22 mV for an increase of 1°C in the $NOCT$, meaning an approximate decrease of the efficiency of 0.5% (Meral and Diner, 2011).

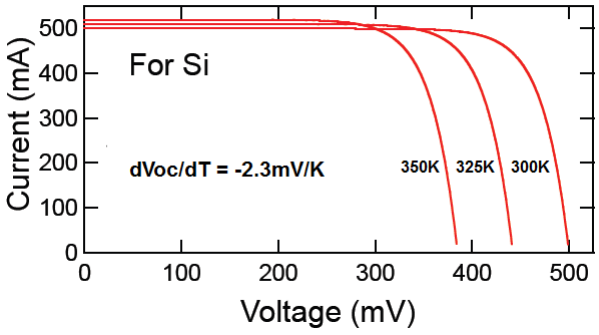

Figure 2.13: Effect of cell's temperature on efficiency (Ahmed, 2020).

2.4.3 Humidity

High levels of humidity on the environment can generate delaminations on the materials that encapsulates solar cells, this can lead to faults on their internal connections and cause efficiency losses due to reduced performance of Isc (Tan et al., 2010; Kempe, 2006).

Humidity can also indirectly decrease the amount of irradiation that solar cells receive. When light rays impact water drops they might be reflected, refracted or diffracted, modifying the direction and amount of energy transmitted by them (Gwandu and Creasey, 1995). For this reason small variations can appear on the Voc and Isc, causing a measurable decrease on the generated energy and the modules efficiency (Mekhilef et al., 2012). Figure 2.14 shows the relation between the irradiation and humidity.

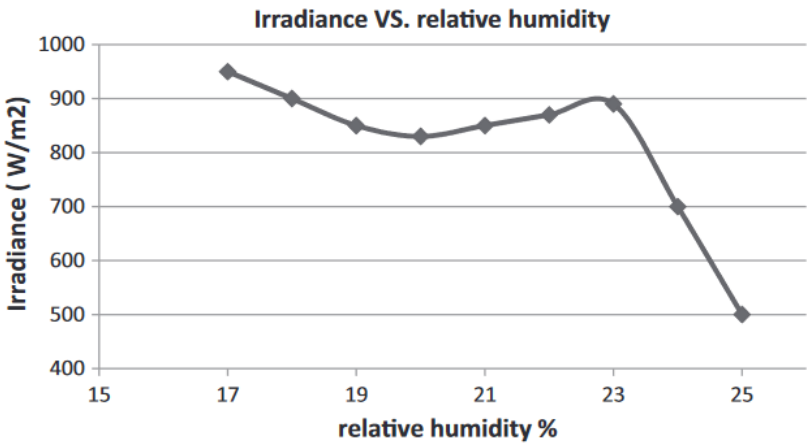

Figure 2.14: Irradiation vs humidity relation (Mekhilef et al., 2012).

2.5 BIPV Technology

BIPV is the integration of PV technologies into the structure of buildings, more specifically on roofs and facades. This kind of technology has been studied and explored as an alternative for electricity generation in urban areas where horizontal available space for traditional PV installations is very limited (Savvides et al., 2019; Vulkan et al., 2018). Figure 2.15 shows the locations at which different studies regarding BIPV have taken place and classifies them into: Grid Integration (10.4%), Building Application and Experimental (34.8%), Simulation and Theoretical (26.1%), Cell/Module Design (16.5%), and Policy and Strategies (12.2%). It is clear that Europe, Asia and the United States are the locations at which most of the researches have taken place. On the other hand, the tropical region of the world (latitudes 23.5°S to 23.5°N) presents a low amount of research done on this topic.

There are three ways of calculating an estimate of the energy generation and performance of this technology. The first one consists on using models like Digital Terrain Model (DTM), Digital Surface Model (DSM), Light Detection and Ranging (LIDAR), Solar Analysis Tool (SAT) and Geographic Information Sistem Model (GIS) (Catita et al., 2014; Cheng et al., 2020; Groppi et al., 2018; Kämpf and Robinson, 2009) to get the irradiance present at the desired location, from this data the amount of energy that could be generated by a solar cell can be calculated. The second option consist on more a experimental approach using actual solar panels or pyranometers to determine the amount of energy that can be generated by the desired surfaces (Díez-Mediavilla et al., 2019; Revesz et al., 2018a). Lastly, using simulations implementing algorithms or software designed specifically for this task, taking into account variables such as the morphology of the building (Ospina-Metaute et al., 2020), the structures where they are located and the conditions of shadow generated by neighboring buildings (Jakubiec and Reinhart, 2013; Brito et al., 2017; Redweik et al., 2013; Hsieh et al., 2013; Jaugsch and Löwner, 2016). Table 2.3 presents different software used for this application and their

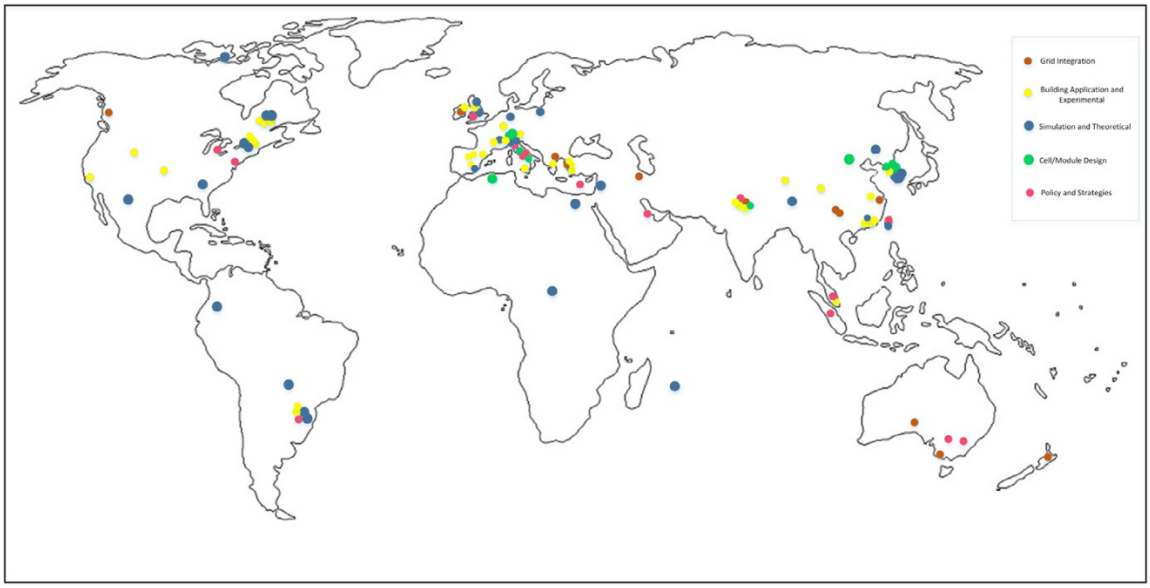

Figure 2.15: Global research on BIPV (Biyik et al., 2017).

individual specialty.

Finally, table 2.5 synthesize some of the previous researches that were made on the BIPV topic, where they were performed and which kind of contribution was made by each work.

Software	Purpose
EnergyPlus	BIPV Analysis and Simulation
Energy3D	Building Thermal Analysis, BIPV Analysis and Simulation
ESP-r	Calculate the power output from the PV system
eQuest	Calculate the yearly electricity usage
CIELAB	Systematic Analysis of Colors
FLUENT	CFD Analysis and Simulation
FORTRAN	Equations and Algorithms Solution
Green Building XML	BIPV Analysis and Simulation
MOSEK	Equations and Algorithms Solution
MATLAB	Equation and Algorithms Solution
PVsyst	PV Modeling and Data Analysis
PHEONICS	BIPV Analysis and Simulation
RETScreen	Annual Electricity Generation
VR4PV	Shadow Factor
TRNSYS	Building Thermal Analysis, BIPV Analysis and Simulation

Table 2.3: Software used in simulation BIPV systems (Biyik et al., 2017).

Author	Year	Location	Contribution
(Ordenes et al., 2007)	2007	Brazil	Potential integration for BIPV evaluating six PV technologies
(Tian et al., 2007)	2006	Mexico	Performance evaluation of BIPV in rural and urban zones, comparing the PV power output and spectral response in both areas
(Rüther and Braun, 2009)	2009	Brazil	Potential energy demand decrease integrating BIPV technologies in Airports buildings
(Yoo and Manz, 2011)	2011	Korea	Power generation analysis in winter through BIPV implementation
(Cronemberger et al., 2012)	2012	Brazil	Solar irradiation potential for different types of surfaces like facades and roofs
(Hwang et al., 2012)	2012	Korea	Relationship between the yearly energy consumption and the yearly energy generation by BIPV in two office buildings
(Pérez-Alonso et al., 2012)	2012	Spain	Development a training method based in ANN to evaluate the efficiency of the BIVP
(Lu and Law, 2013)	2012	China	Development of a methodology to estimate the overall energy performance of semitransparent, single glazed PV window
(Yang and Athienitis, 2014)	2014	Canada	Mathematical model for a BIVP system with one and two inlet to determinate the thermal efficiency and the peak module temperature
(Veldhuis and Reinders, 2015)	2015	The Netherlands	Analysis of shadows effects on BIPV systems
(Elsayed, 2016)	2016	Egypt	Methodology to determinate the optical air gap for BIPV systems

Table 2.4: Simulation and numerical studies.

Author	Year	Location	Contribution
(Yang et al., 2004)	2004	China	Experimental study of the performance and efficiency for a BIPV system with air gap for cooling purposes
(Jiménez et al., 2008)	2008	Spain	A methodology development for linear and non linear continuous time modeling of physical systems using discrete time data
(Agrawal and Tiwari, 2011)	2011	India	Thermal model and analysis under climatic conditions for a BIPV system in two cities
(Vats and Tiwari, 2012)	2012	India	Study the performance of semitransparent and opaque BIPVT systems for roofs and facades considering air duct and without air duct
(Peng et al., 2011)	2011	China	Architectural design aspects for BIPV systems, considering the lifetime, maintenance and replacement of PV components
(Santos and Rüther, 2012)	2012	Brazil	Potential evaluation of BIPVs for residential buildings
(Drif et al., 2012)	2012	Spain	A method to evaluate the energy losses related to partial shading of BIPV systems
(Ritzen et al., 2015)	2015	The Netherlands	Evaluation of BIPV to buldings, price decline, efficiency and electrical storage
(Chen and Yin, 2016)	2016	USA	BIPV system design to cooling the module solar with water

Table 2.5: BIPV application previous researches.

Chapter 3

Proposal

This chapter describes the design of the devices and experiments that were developed during this study. Section 3.1 presents the development of a device that, in contrast with those found the literature and commercial review made in chapter 2, uses a simplified method to compare the performance of solar cells that are exposed to different orientations and optical conditions by measuring their Isc and Voc. Section 3.4 describes the experiments performed to evaluate the behavior of vertical BIPV in tropical regions.

3.1 Simplified method to evaluate the performance of solar modules

The idea of developing and implementing a method to evaluate solar cells under different orientations and optical conditions originates from the development of the solar brick, a BIPV power generating device for vertical facades developed at Universidad EAFIT (Velasquez-Lopez et al., 2014; Betancur et al., 2016). One of the main functional parts of these bricks is the optical cover. These covers are designed to maximize the amount of solar rays that reach the surface of the vertical solar cells and thus increase the energy generation. Figure 3.1 presents an example of three optical covers, in this case, a triangular cover (on its cross section) and two flat covers made of different materials are presented.

The design process of these covers starts by using mathematical models to find the most appropriate shapes and materials to optimize the amount of rays reaching the cells. Prototypes are then manufactured and tested, this is where a method to evaluate their performance would be essential as a validation process to the effectiveness of each prototype. In addition to this, and as discussed in the state of the art, the orientation of the solar modules is one of the most critical variables when trying to maximize the energy generation, a method to identify how the solar bricks and covers would

perform under different orientations would also be critical for the optimization of these systems.

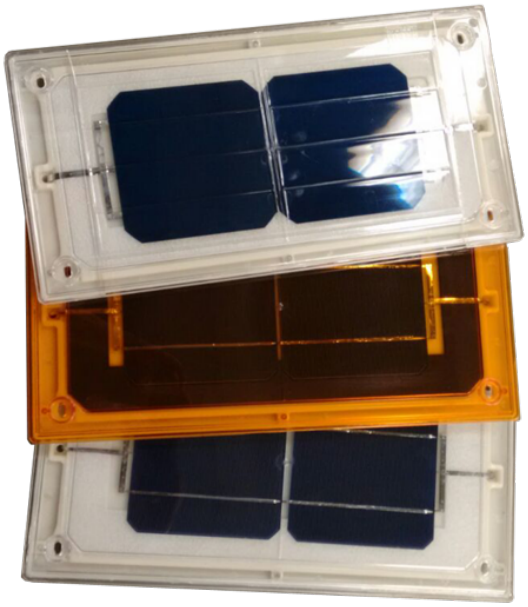

Figure 3.1: Solar brick's optical covers.

After evaluating the state of the art of devices capable of measuring the performance of solar cells a common problem was encountered between them, they are designed to evaluate only one cell at a time. Since in the case of the solar bricks the performance evaluation was meant to be performed under real working conditions instead of under controlled lab environments, the method to be used required a device capable of evaluating multiple solar bricks simultaneously so that the meteorological conditions were exactly the same for all the modules at the time of the measurements. For this reason the design, prototyping and implementation of a new device was necessary to meet these requirements.

The device was designed with the goal of comparing several equal solar cells under different optical conditions and orientation to determine which one presents the best energy performance. As described in section 2.2, the power generated by a solar cell can be defined as a function of the Voc, Isc and FF as shown in equation (3.1)

$$P_{MaxOut} = V_{OC} * I_{SC} * FF \tag{3.1}$$

Considering that the solar cells to be evaluated are the same reference and are operating under the same climatic conditions their FF can be considered to be equal. As explained in section 2.4 the FF depends on the temperature (Qu and Li, 2019), irradiance (Cuce et al., 2013) and the materials and manufacturing process of the cells (Reusch et al., 2013). In this case we would be making all these variables equal and thus the FF of the cells would be the same.

As shown in equation (3.2), by considering an equal FF for the cells to be compared, it is possible to determine which cell generates more energy and get an approximation of the real energy generation of each cell from the measurement of the Voc and the Isc. In this case, E_{ratio} represents the relationship between the energy generated by both cells.

$$E_{ratio} = \frac{\int_{t_i}^{t_f} P_{C1}dt}{\int_{t_i}^{t_f} P_{C2}dt} = \frac{\int_{t_i}^{t_f} FF_1 * V_{OC1} * I_{SC1}dt}{\int_{t_i}^{t_f} FF_2 * V_{OC2} * I_{SC2}dt} = \frac{\int_{t_i}^{t_f} V_{OC1} * I_{SC1}dt}{\int_{t_i}^{t_f} V_{OC2} * I_{SC2}dt} \tag{3.2}$$

It is important to clarify that the "Energy" being calculated with equation 3.2 does not correspond to the MPP nor any point of the IV curve but to the point P_{IV} from image 2.2, which is strictly being used for comparison purposes and is an indirect measurement of the real energy generation capacity of the cells.

By applying the described method of using Voc and Isc to evaluate solar cells, it becomes possible to make fast and precise measurements of their performance while at the same time reducing the complexity of the hardware being used. This would allow reaching the goal of taking measurements on a small time frame to keep the same climatic conditions for the cells being evaluated.

The specifications of the solar brick's solar cells were an essential input for the design process of the proposed device. The bricks consists of two modules of Mono-Crystalline C60 solar cells manufactured by SunPower connected in series, each with a maximum voltage of 0.58V, an output power of 3.42W and an efficiency of 23%.

The following sub-sections will present the design, prototyping and testing of the different versions of the device, versions two and three were the ones developed under this project.

3.1.1 Version One

During the year 2018 the first prototype of the device was developed. This design implemented the Hall-Effect Sensor $WCS1800$, with a measuring range from -35A to 35A, for the measurement of Isc. An Arduino UNO was used to read the data from the sensor and was also in charge of measuring Voc by using one of its analog pins. An SD card Arduino shield was used to store the collected information for further analysis in a computer. Finally a relay was used to open and short the circuit to switch between the current and voltage measurements. Figure 3.2 present the prototype layout and circuit schematic. For this prototype two multimeters were incorporated into the electric circuit to verify the measurements taken by the Arduino and Hall sensor. This initial approach to the circuit was design to only measure one cell at a time.

3.1.2 Version Two

The development of the second version began in 2019. This time the main objective was to expand the amount of cells that could be evaluated at the same time. To do this, a set of eight relays were

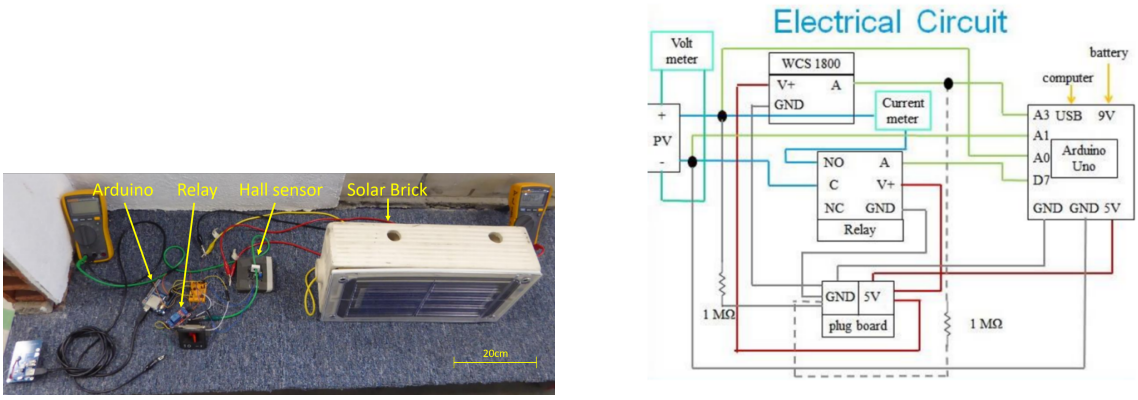

(a) Prototype.

(b) Prototype schematic.

Figure 3.2: Prototype version 1 layout (Stephan, 2019).

connected to a multiplexer controlled by the Arduino. These were able to evaluate four cells at a time by closing the circuit of the cell being measured at a specific period of time, while keeping the others disconnected from the measuring hardware. Once the measurement of a cell was completed it would be disconnected and the next one would connect to the circuit to be tested. This cycle would continue until the four cells were evaluated.

In addition to this the Isc measuring hardware was changed for a sensor that better suited the ranges in which the solar bricks work, section 3.1.2.2 present further information on the selected sensor. Another major change was the implementation of Internet of Things (IoT) for data storage and analysis by including a Wi-Fi module connected to the Arduino and to an online cloud-based IoT dashboard. Subsections 3.1.2.1 to 3.1.2.4 describe in more detail the individual subsystems and components used in version two.

3.1.2.1 Control

This subsystem controls the measurement equipment, acquires and saves the data. An Arduino Uno was selected for this task due to its availability, versatility and low price. It also incorporates all the necessary hardware such as analog inputs, digital inputs/outputs and compatibility with a vast list of sensors.

As mentioned before, the goal of the device is to compare the performance of various units of the same solar cell with different optical covers and orientations, reason why a multiplexed system was integrated into the device. In order to address multiple cells at the same time, they are connected to a series of relays that are controlled by the Arduino; this way it is able to control which cell is being evaluated at a certain instant of time. Since only Voc and Isc are being measured, each cell

can be evaluated in less than 500 millisecond. As stated in chapter 2, the time frame in which the measurements are taken has to be as short as possible to maintain a stable irradiance, temperature and obtain reliable data. After checking each cell, the Arduino switches the relays that correspond to the next one; thus the cycle continues until the last cell is evaluated. A timer controls the interval between each set of measurements.

3.1.2.2 Measurement

Two separate systems were designed to acquire the values of Voc and Isc.

Open-Circuit Voltage

One of the analog pins of the Arduino was used to measure Voc. In order to utilize the entire range of sensitivity of this pin (Max. 5V with a 4.9mV resolution) and to ensure that the signal was more reliable, an operational amplifier was used. A Non-inverting configuration was set on the amplifier to generate a gain on the voltage generated by the cell, this configuration is shown in Figure 3.3a.

Short-Circuit Current

The current sensor ACS711EX, made by Pololu, was used to measure Isc. This sensor has a working current range between -15A and 15A, is electrically centered at 2.5V when the measured electric current is zero and has a gain of 136 mV/A. As complement to this sensor, one voltage divider and two operational amplifiers were used. The first amplifier was configured as a subtractor (Figure 3.3b), it was connected to the sensor and to the voltage divider in order to re-center the input signal at 0V since no negative currents were going to be measured. The second operational amplifier was configured as Non-inverting and set to a gain that allowed connecting it to an analog input of the Arduino where the measurement was made and saved.

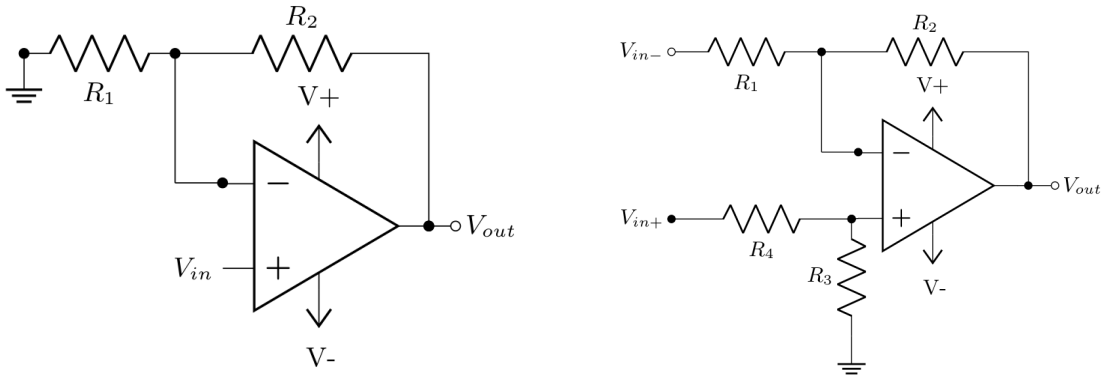

(a) Non-inverting Operational Amplifier.

(b) Differential Amplifier.

Figure 3.3: Implemented Operational Amplifiers.

3.1.2.3 Communication

This subsystem was responsible for sending the acquired data to the IoT platform. In this case, an ESP8266 module, made by Espressif, was used for the communication. This device is capable of connecting to a Wi-Fi network and establishing communication with an online server.

The ESP8266 was connected to the Arduino UNO through Serial communication enabling data sharing between both devices. Specifically, the Arduino UNO sends data to the ESP8266 every time new measurements are acquired. After reading the data, the ESP8266 sends a HTTP request to the IoT server, where the data can be seen in real time, plotted and analyzed. The IoT platform Ubidots was used for this version of the device, mainly due to its easy setup and user friendly interface. The platform also allows downloading the acquired data into a CSV file for further research and analysis.

3.1.2.4 Code

The Arduino UNO and the ESP8266 module were programmed using the Arduino IDE which is an open source program based on the C++ programming language released and supported by Arduino. Figure 3.4 shows a flowchart of the implemented algorithm. The code developed for the Arduino consists of six sections, each responsible for each block shown in the flowchart. The ESP8266 only handles the last block which corresponds to the interaction with the IoT platform.

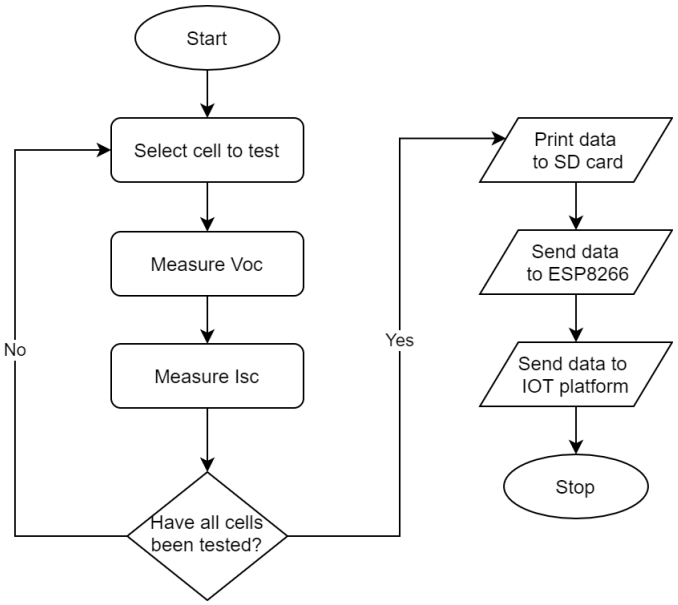

Figure 3.4: Algorithm's flow diagram.

The first section defines the cell to be evaluated in the current cycle, after that Voc and Isc are measured for the selected cell. This cycle repeats until all the cells are evaluated. The rest of the

sections are in charge of the following functions: writing data to the SD card (if present) and sending data to the ESP8266.

The ESP8266 is always waiting for communication from the Arduino. After the information is received it organizes it on the structure needed by the IoT platform and sends it via HTTP communication. Ubidots, the platform that was used to store the information from this device, has an specific library implemented for this microcontroller. This library is in charge of safely sending the data through HTTP protocol making use of the personal API keys generated by Ubidots' dashboard.

3.1.3 Device prototyping

The developed device is presented in Figure 3.5.

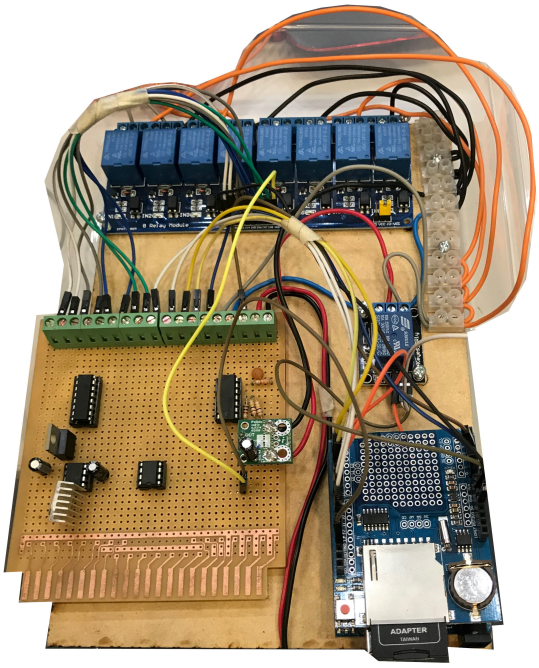

Figure 3.5: Second circuit prototype.

One minor change was made to the circuit after some initial testing. Initially it was necessary to have positive and negative voltage power sources which was not ideal as batteries were expected to be used as the main power source for the device. For this reason, new amplifiers that could work without negative voltages were implemented, Figure 3.6 presents the new universal board design, which only differs from the previous one on the amplifiers used. Figure 3.7 presents the detailed electronic schematic of the connections and distributions of the components. Finally, table 3.1 contains the references, amount and price of the electronic components used.

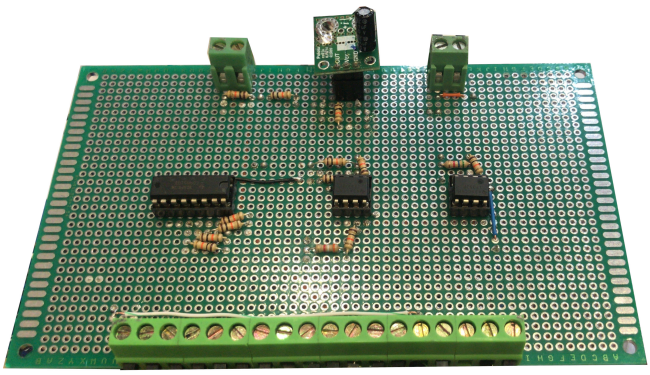

Figure 3.6: New multiplexing circuit for version 2.

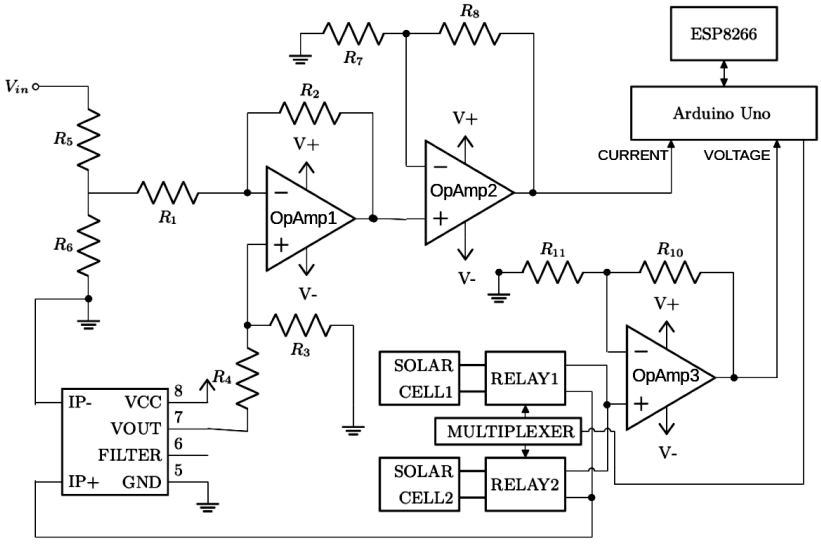

Figure 3.7: Prototype schematic.

3.1.4 Initial tests

Two tests were set up in order to evaluate how well the device would operate comparing the performance of a solar cell under different conditions.

The first test was used as a control group for validation. For this initial setup two generation modules of the solar brick were used. As mentioned before, these modules consist of two Mono-Crystalline C60 solar cells connected in series each with a maximum voltage of 0.58V, an output power of 3.42W and an efficiency of 23% (see Figure 3.8). The modules were placed beside each other, in vertical position with an azimuth angle of 220° as shown in Figure 3.9. Since this test was for verification purposes, the measurements were taken with a time interval of one minute during an hour, in this case the expected result was getting similar, if not identical, readings for Isc and Voc for both modules.

Element	Ref	Units	Price (USD)
Arduino	Uno	1	23.00
Multiplexer	CD4051	1	0.58
Current Sensor	ACS711	1	9.95
8 Channel Relay Board	-	1	8.99
Operational Amplifier	LF353	2	2.06
Module GSM	ESP8266	1	2.14
Resistor	-	10	0.39
Extras	-	-	10.82
Total	-	-	57.93

Table 3.1: Elements used in the developed device.

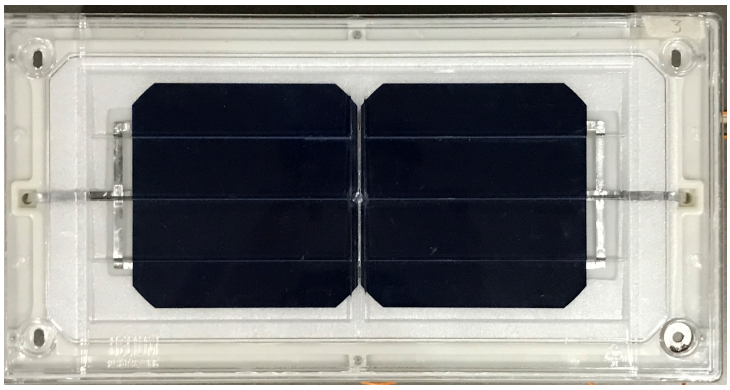

Figure 3.8: Module used in the test.

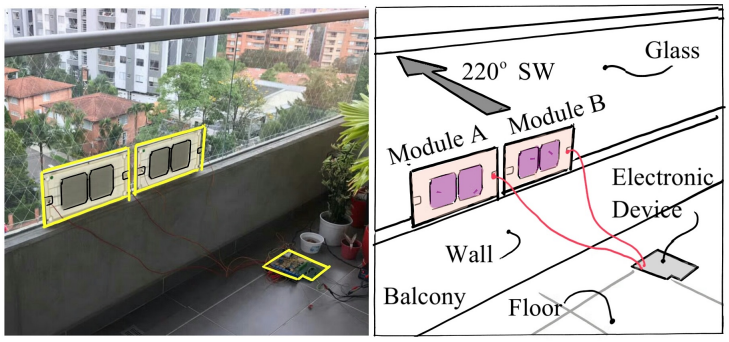

Figure 3.9: Layout of test 1.

For the second test, the same modules were used and the main goal was to compare their performance by changing their orientation. One module was placed vertically, with an azimuth angle of

220°, while the other was placed horizontally. The test setup is presented in Figure 3.10. The time interval between measurements was set to five minutes and the total operating time from 5am to 7pm in order to have data for an entire day. The test was performed on the 9th of May of 2020.

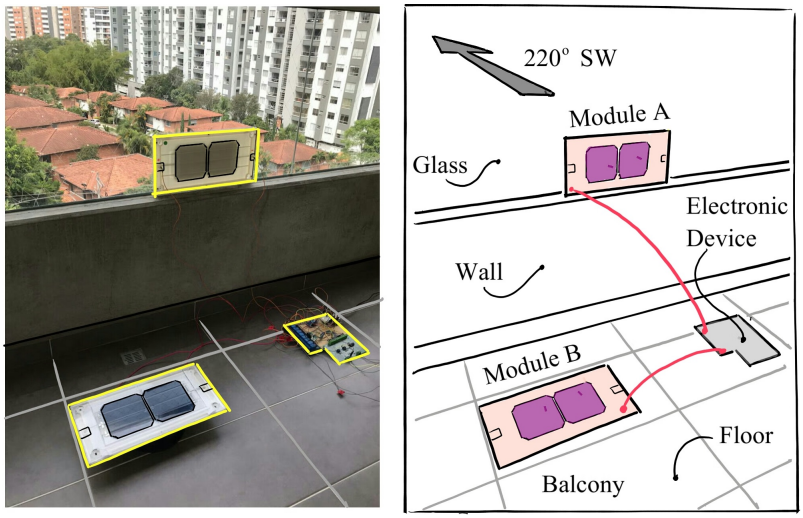

Figure 3.10: Layout of test 2.

Tables 3.2 and 3.3 synthesize the conditions presented for both experiments.

Module	Solar Cell	Cover	Back-sheet	Position	Azimuth
A	Mono-Crystalline	Triangular-Transparent	White	Vertical	220°
B	Mono-Crystalline	Triangular-Transparent	White	Vertical	220°

Table 3.2: Test 1 setup: Validation for the same position.

Module	Solar Cell	Cover	Back-sheet	Position	Azimuth
A	Mono-Crystalline	Triangular-Transparent	White	Vertical	220°
B	Mono-Crystalline	Triangular-Transparent	White	Horizontal	-

Table 3.3: Test 2 setup: Comparison by varying position.

3.1.5 Results

The first test's results show the same behaviour for both modules, having close to identical Isc and Voc curves (Figure 3.11). This result suggests that both modules responded equally to the environmental conditions, behavior that is expected for two sets of the same module positioned facing the same orientation.

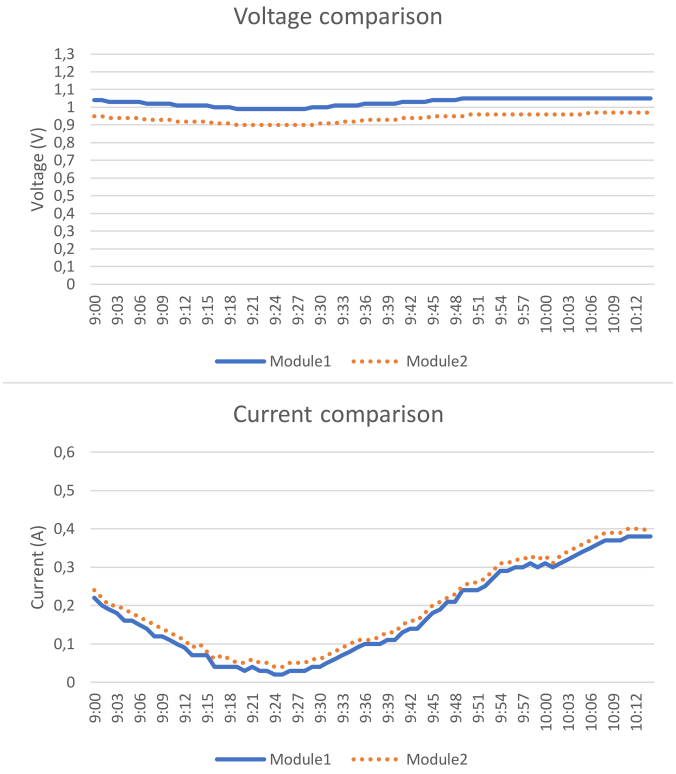

Figure 3.11: Results of test 1.

The results of the second test are shown in Figure 3.12. The graphs show that the behaviour of Voc for both modules is similar, having no peaks and being almost constant throughout the day. Isc, on the other hand, showed clear differences. This behavior was expected as the Isc has a direct relation with irradiance, while the Voc presents a logarithmic relation (C.B.Honsberg, 2019).

Figure 3.13 presents both modules' Isc for comparison. The vertical module has a faster increase in current, with a first peak at 7:30am and a maximum peak at 2:30pm. As for the horizontal module, the Isc curve stays low until 10:15am and reaches its maximum peak at 2:45pm.

By following the proposed methodology, the performance of the solar cells was compared using Isc and Voc. The results are shown in table 3.4, where the maximum values are presented, as well as the summatory of Isc which gives a more objective look of the performance over time.

Module	**Solar Cell**	**Position**	I_{sc} **Max (A)**	V_{oc} **Max (V)**	I_{sc} **in time (Ah)**
A	Mono-Crystalline	Vertical	0.52	1.05	3.23
B	Mono-Crystalline	Horizontal	0.48	0.96	1.84

Table 3.4: Results of test 2 setup.

By replacing the acquired data on equation 3.2, the ratio between the maximum instantaneous

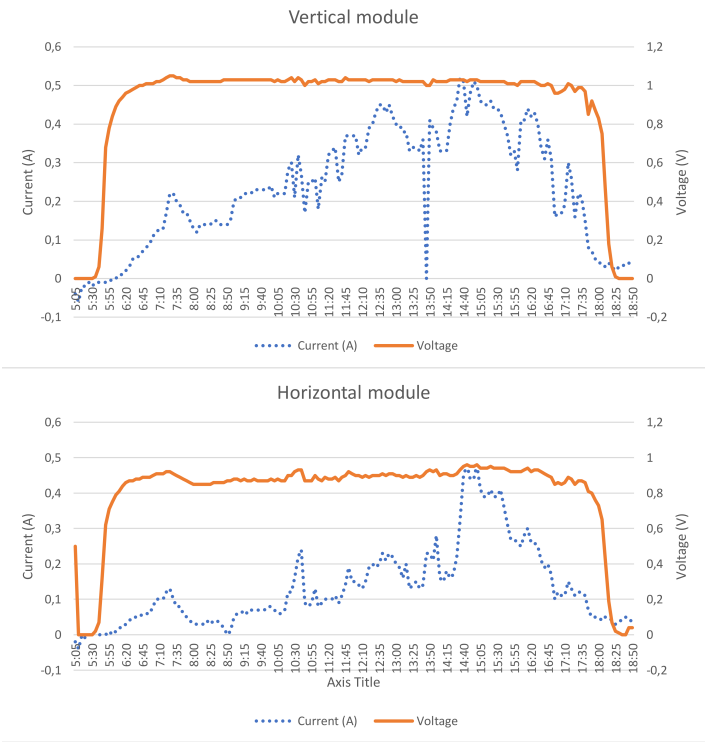

Figure 3.12: Performance of the vertical and horizontal modules.

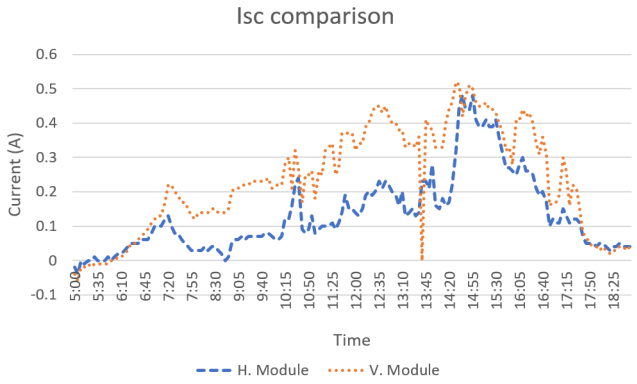

Figure 3.13: Modules Isc comparison.

power of the solar cells, P_{ratio}, is calculated.

$$P_{ratio} = \frac{\int_{t_i}^{t_f} V_{OC1} * I_{SC1} dt}{\int_{t_i}^{t_f} V_{OC2} * I_{SC2} dt} = \frac{2.91}{1.65} = 1.76 \tag{3.3}$$

Figure 3.14 shows the energy generated over time for both modules. It is important to note, as previously explained, that the energy calculated by multiplying Voc and Isc represents an approximation to the real energy generated by the solar modules. This graph suggests that the vertical module

had a better performance in this test, as its results are 76% higher (Eqn. 3.3) than the one of the horizontal module.

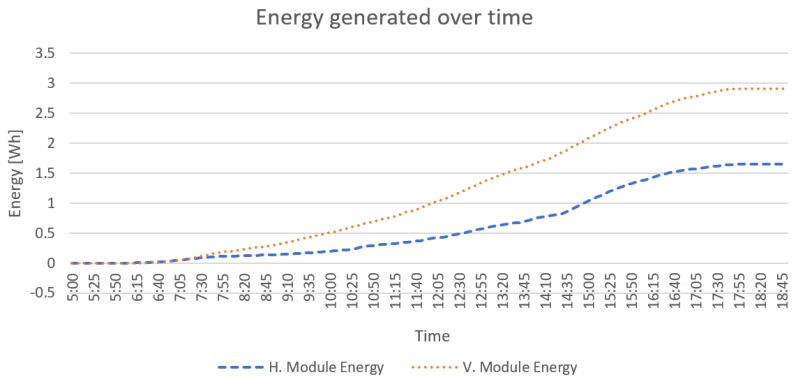

Figure 3.14: Modules energy comparison.

This atypical behaviour (normally horizontal modules have better performance than vertical modules) is explained by the set up of the test. Due to the place where the horizontal module was located, it did not have access to direct sunlight except for a small time gap between 2:30pm and 4:00pm. On the other hand, the vertical module had access to direct sunlight after noon. In addition to this, the horizontal panel also had less access to indirect light in comparison with the vertical that was located in front of a window. These test related variables caused the vertical module to perform better. Its important to notice, however, that these experiments were performed just as a test of the performance of the device and no conclusions about the real performance of the cells were made from them.

3.2 Version Three

With the experience gained from the tests made with the second version of the device, five items were found to have improvement potential. The items found and the modifications made for version three are as follows:

1. The module ESP8266 was changed for a GSM module compatible with Arduino, the module used was a $SIM900\ GSM$, which connects to a mobile network and establishes the connection and data transfer with the online server. The module connects to the Arduino through serial communication and uses the HTTP communication protocol to send information to the IoT platform. The main advantage of this module over the ESP8266 is that it does not require to be close to a Wi-Fi source and can be used from anywhere with a cellular network available, this way experiments can be made virtually anywhere in the country.

2. The current sensor $ACS711$ was replaced by a sensor $ACS714$, manufactured by Pololu. This

sensor has an operating range from -5A to 5A, is centered on 2.5V and has a gain of 185 mV/A. Since it has an operating range smaller and a higher gain, the resolution of the sensor is better and allows more precise measurements.

3. The relays were replaced by MOSFETs reference $IRN1010N$, which are still controlled by the Arduino though a multiplexer to select the cells to be evaluated. The transistors allow evaluating each cell in a time shorter than 200ms and increase the expected life span of the device as they do not have mechanical parts. In addition to this, the MOSFETs work quietly, which would be beneficial in case of making experiments in working or living areas.

4. The device was initially assembled on breadboard, however, its design was improved and mounted on a PCB, reducing its size and eliminating noise generated by soldering and wiring.

5. The IoT platform was changed to ThingSpeak. The main reasons for changing the platform were limitations of the previous one (Ubidots). Firstly, it would not allow to download large amounts of data at the same time. Secondly, the allowed amount of daily data to upload to the platform was also restricted. ThingSpeak's free account, on the other hand, is limited to 3.000.000 data uploads per year, which is more than enough for the needs of this study. It also allowed unlimited data downloads.

The rest of the device remained the same as described in section 3.1.2.

Figure 3.15 presents the schematic of the electrical connections between the components of the final device, only two solar modules are shown as demonstration but the device still evaluates up to four modules at a time. Figure 3.16 presents the design of a 2-layer PCB and a render of the device. Table 3.5 contains the references, quantity and price for the different components of the circuit. Finally, Figure 3.17a presents the prototype made for this version and Figure 3.17b the final product assembled on the designed PCB.

3.2.1 Validation

In order to validate the instrument, a SOLAR-600 IV curve tracer was used. Both devices were connected to the same solar cell and programmed to take measurements every minute. A total of 129 points were acquired for this test. The data acquired from both devices was saved and processed in order to check its matching. Figures 3.18a and 3.18b show the scatter plots that were obtained after mapping the instrument's and SOLAR-600's measurements.

The validation test shows that the coefficient of determination (R^2) is 0.9981 and 0.9866 for Isc and Voc respectively, meaning that the relation between the device's and SOLAR-600's Voc and Isc measurements is strong. In addition, and as expected, the equations of the lines that describe the

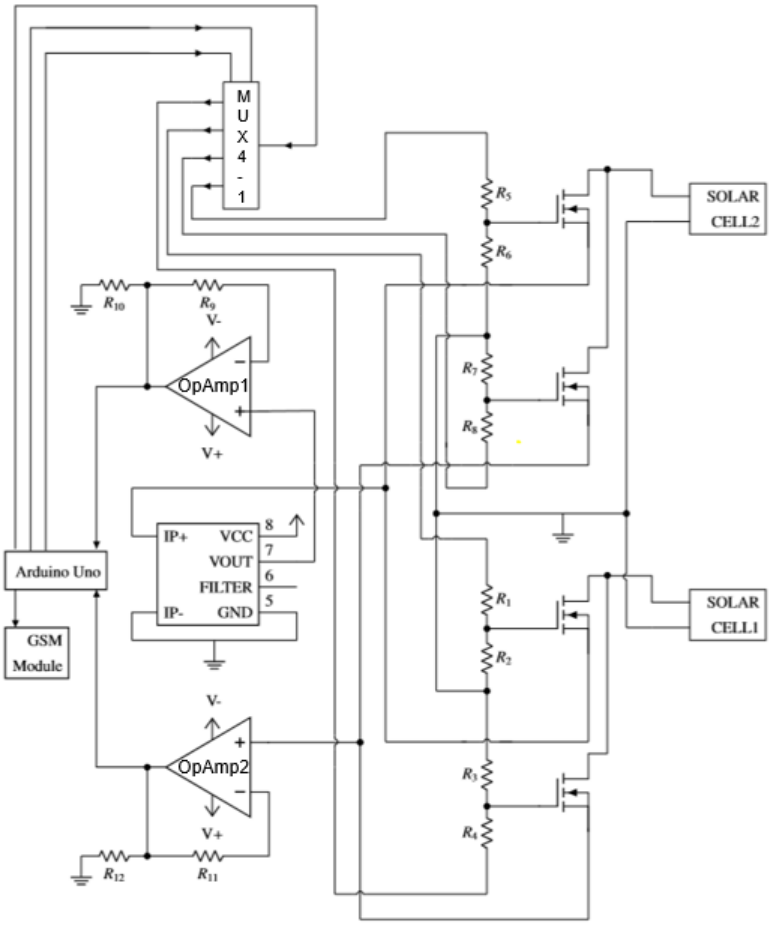

Figure 3.15: Final prototype schematic.

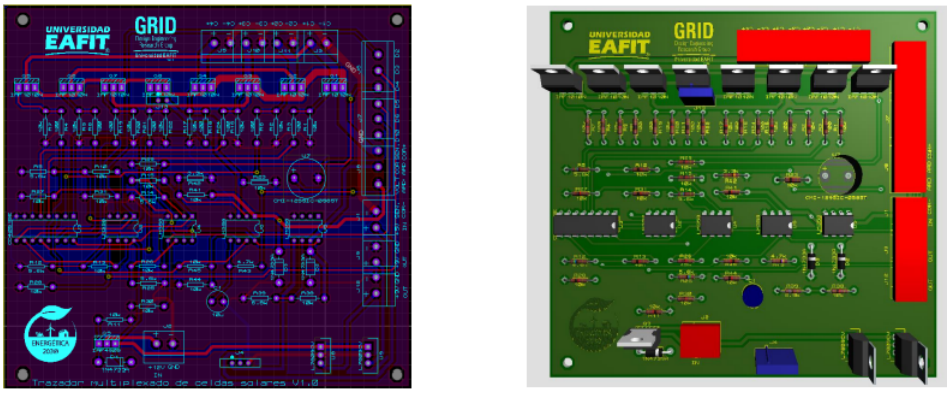

Figure 3.16: PCB design.

correlation between both devices are close to $Y = X$, meaning their measurements are close to being equal.

Element	Ref	Units	Price (USD)
Arduino	Uno	1	23.00
Multiplexer	CD4051	1	0.58
Current Sensor	ACS725	1	9.95
MOSFET	IRF1010N	8	11.52
Operational Amplifier	LF353	2	2.06
Module GSM	SIM500	1	59.90
Resistor	-	38	4.94
PCB	-	1	32.8
Extras	-	-	10.82
Total	-	-	155.57

Table 3.5: Elements used in the developed device.

3.2.2 Test Setup

As with the device's previous versions, a set of tests were planned and implemented to evaluate how the device would perform under real experimental conditions. Two experiments were set up at Universidad EAFIT (Medellin, Colombia) in order to compare the performance of solar cells with different optical covers and orientation. Each experiment evaluated four cells facing the same azimuth angle, two of which had flat covers while the other two had triangular cross section covers. Figure 3.19 presents a picture of both profiles used. For both experiments the time interval between measurements was set to one minute and the operating time was three days, for a total of six days for both experiments.

The tests setup and results obtained on the following sections of the study were presented at the international conference WEA 2020. (Giraldo-Pérez et al., 2020)

3.2.2.1 Optical variation

Four solar brick modules were used. Two had a flat front cover, while the other two had a triangular profiled front cover, Figure 3.20 shows the four modes used for the tests.

The modules were placed beside each other, in vertical position with an azimuth angle of 286° so that they receive direct sunlight during the afternoon as shown in Figure 3.21a. The test's conditions are synthesized in Table 3.6.

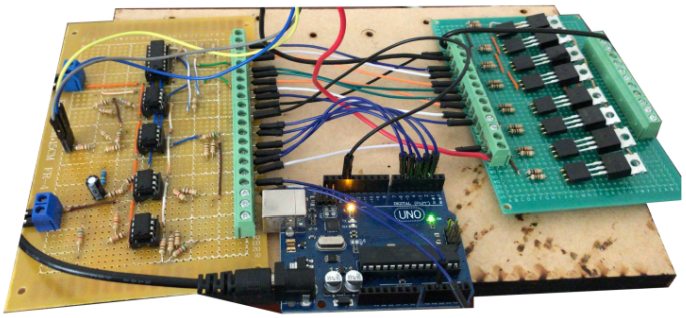

(a) Final circuit assembled on an universal board.

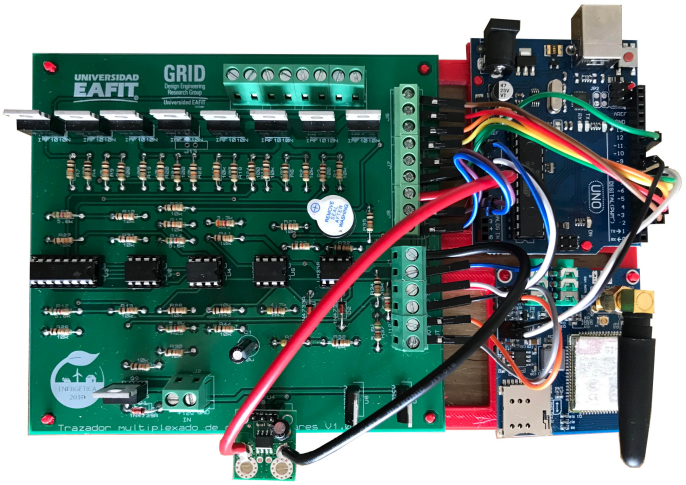

(b) Final circuit assembled on a printed PCB.

Figure 3.17: Initial and final versions of the device.

Module	Solar Cell	Cover	Back-sheet	Position	Azimuth
A & B	Mono-Crystalline x2	Flat-Transparent	White Foam	Vertical	286°
C & D	Mono-Crystalline x2	Triangular-Transparent	White Foam	Vertical	286°

Table 3.6: Test 1 setup, comparison of different front covers.

3.2.2.2 Orientation variation

The same modules were used for the second test. The objective was to change their orientation to evaluate and compare their performance with the results obtained in the previous test. In this case the modules were rotated 180° so that the cells received direct radiation in the morning as shown in Figure 3.21b. Table 3.7 synthesizes the conditions presented for this test.

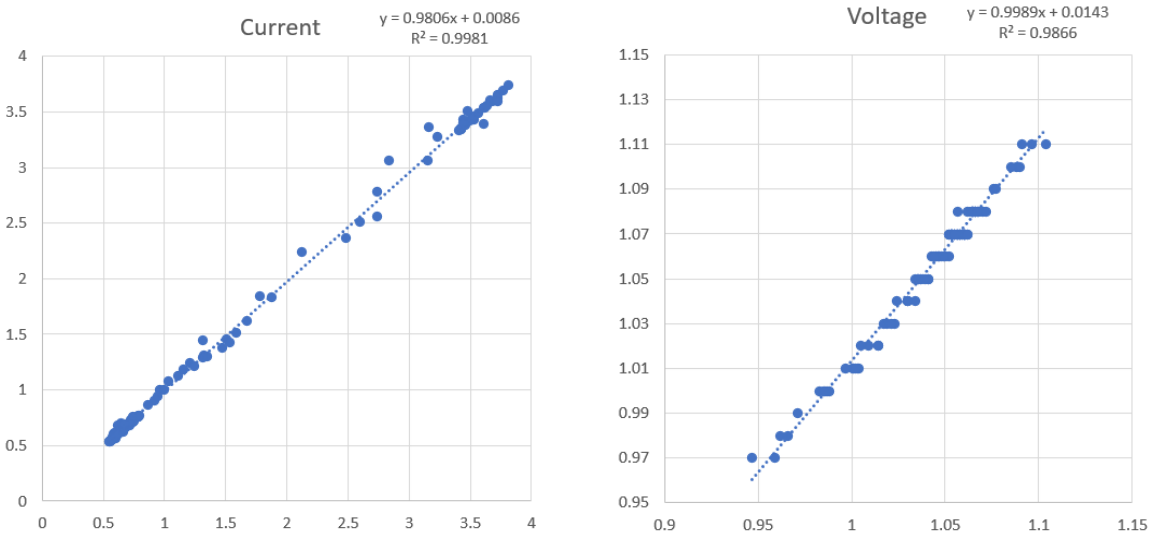

(a) Scatter plot of Isc taken with SOLAR 600 (X axis) and the device (Y axis).

(b) Scatter plot of Voc taken with SOLAR 600 (X axis) and the device (Y axis).

Figure 3.18: Voltage and current measurement validations.

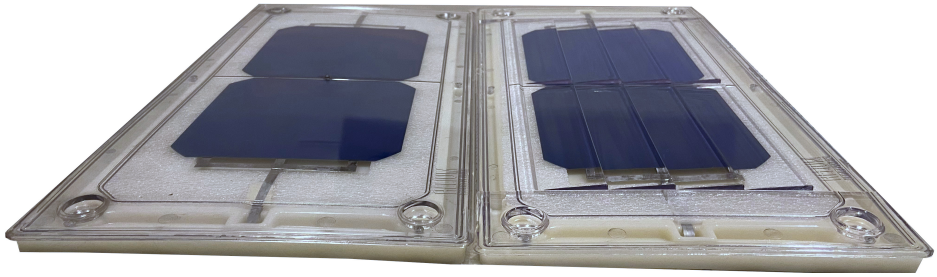

Figure 3.19: Flat and triangular profiles.

Module	Solar Cell	Cover	Back-sheet	Position	Azimuth
A & B	2 X Mono-Crystalline	Flat-Transparent	White Foam	Vertical	106°
C & D	2 X Mono-Crystalline	Triangular-Transparent	White Foam	Vertical	106°

Table 3.7: Test 2 setup, comparison of different orientations.

3.3 Results

A total of 8606 points were retrieved from the IoT platform, each containing the measurements of Voc and Isc for each module. Table 3.8 synthesizes the results for both experiments after integrating the product of Voc and Isc over time to get an approximation of the energy generated by the modules. The results were divided into two categories, one comparing the performance of the cells with different

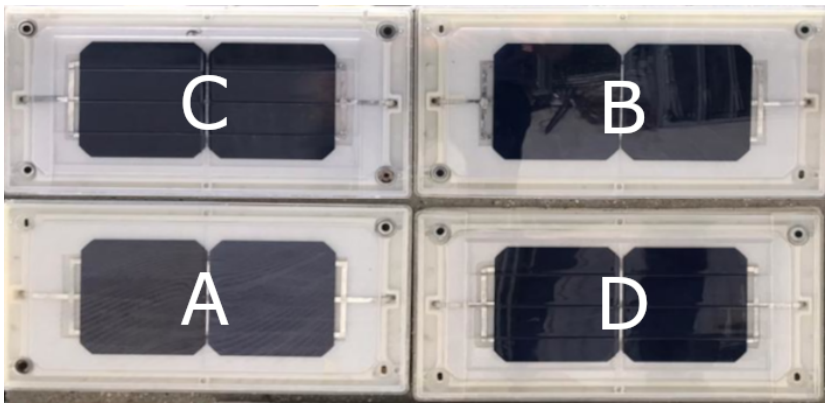

Figure 3.20: Modules used in the test.

(a) Test 1, 286° orientation.

(b) Test 2, 106° orientation.

Figure 3.21: Implemented Experiments.

optical profiles and the other one comparing the performance under different orientations.

Module	Energy (Wh)		Total Energy (Wh)	Relationship between test 1 and test 2
	test 1	test 2		
A	49.02	42.19	91.21	1.16
B	46.68	39.07	85.75	1.19
C	42.32	35.06	77.38	1.20
D	44.17	37.18	81.35	1.18

Table 3.8: Results of experiments 1 & 2.

Figure 3.22 shows an example of how the voltage and current graph looks for each module on each test. As expected, Voc remains constant throughout the day time of the experiments while Isc

changed as a function of irradiance. On test 1 (modules with an azimuth of 286°) the Isc stayed bellow 1A during the morning, and after 12:00pm, when the sun's irradiance directly reached the cells, the Isc increased up to 4.8A. Test 2 showed an opposite behaviour, since the Isc peak occurred in the morning, and after 12:00pm it remained below 1A.

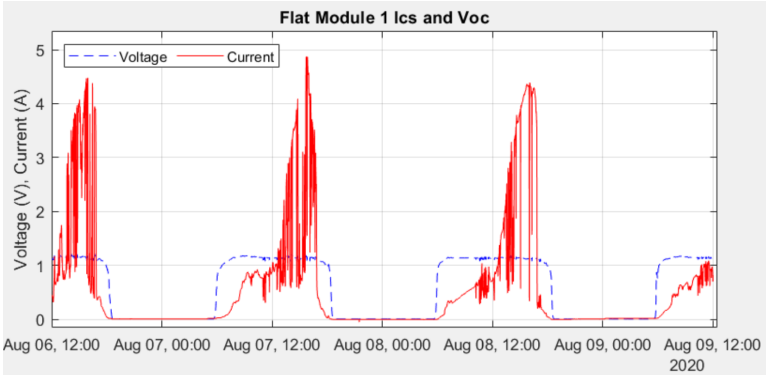

(a) Module A, test 1.

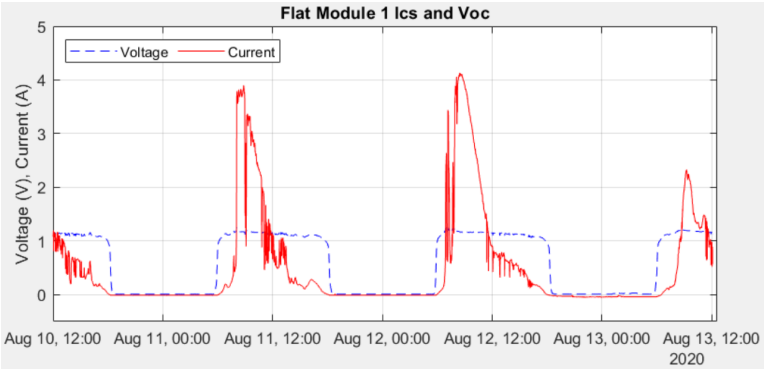

(b) Module A, test 2.

Figure 3.22: Isc and Voc vs time curves - Module A.

3.3.1 Influence of the optical profile

The measurements obtained by the device gave evidence of the differences of the overall energy generated by the two types of optical profiles under study.

The overall differences in power generation indicate that, as shown in equation 3.4, the flat optical profile (Modules A & B) was 11.5% more efficient than the triangular profile (Modules C & D) for both experiments. That is, the sum of the energy generated by the modules with the same optical profile shows that the flat modules generated a total energy of 176.96 Wh while the triangular generated 158.73 Wh.

$$E_{ratio} = \frac{\int_{t_i}^{t_f} P_{flat} dt}{\int_{t_i}^{t_f} P_{triangular} dt} = \frac{176.96\ Wh}{158.73\ Wh} = 1.115 \tag{3.4}$$

3.3.2 Influence of orientation

To identify the influence of orientation equation 3.2 was used. In this case, as the optical covers were not be taken into account, results of all modules for each test were added and then compared. During Test 1 a total of 182.19 Wh was generated, while the value achieved during test 2 was 153.5 Wh.

$$E_{ratio} = \frac{\int_{t_i}^{t_f} P_{exp1} dt}{\int_{t_i}^{t_f} P_{exp2} dt} = \frac{182.19\ Wh}{153.5\ Wh} = 1.187 \tag{3.5}$$

The ratio result indicates that test 1 was 18.7% more efficient, meaning that for this case the azimuth angle of 286° was better for vertical solar energy harvesting compared to the 106° angle.

3.4 Test design and preparation

After the final version of the circuit explained in section 3.2 was manufactured and tested the preparation for the principal experiments began. The objective of such experiments was to directly assess the research questions of the study. To do this, the experiments required evaluating the performance of both vertical and horizontal BIPV modules. The fist step was selecting the solar modules to be used. In this case, as the prototypes were tested using Universidad EAFIT solar brick modules, they were again chosen to perform the experiments as they have electrical characteristic compatible with the circuit and were designed to be part of BIPV installations.

The second stage of the preparation consisted on designing a setup where the modules could be placed in the desired orientations. Figure 3.23 presents the final concept consisting of a structure made of acrylic and 3D printed parts. It was designed to fit four solar brick modules. Two modules were positioned horizontally for control reasons, this way the measuring hardware can be monitored as those two should always get close to the same measurements. The design also included a detachable box to fit all the necessary electronics and keep them safe from the sun and rain.

Two cities located in Colombia were chosen as representatives of the tropical zone, a roof top in the city of Envigado (06°10′41.8″N 75°34′23.4″W, Elevation: 1640m) and Universidad EAFIT's subsection in Llanogrande (06°06′21.0″N 75°27′25.1″W, Elevation: 2151m). Each location was used for independent experiments. As for the vertical orientations, east and west were selected due to the sun path throughout the year in this region as suggested by (Ghazali et al., 2017).

It is important to clarify that the locations were selected by convenience. In an initial location evaluation, Llanogrande and Universidad UPB in Medellin were found to be optimal specially due to the availability of meteorological stations on both locations. However, the study was performed in

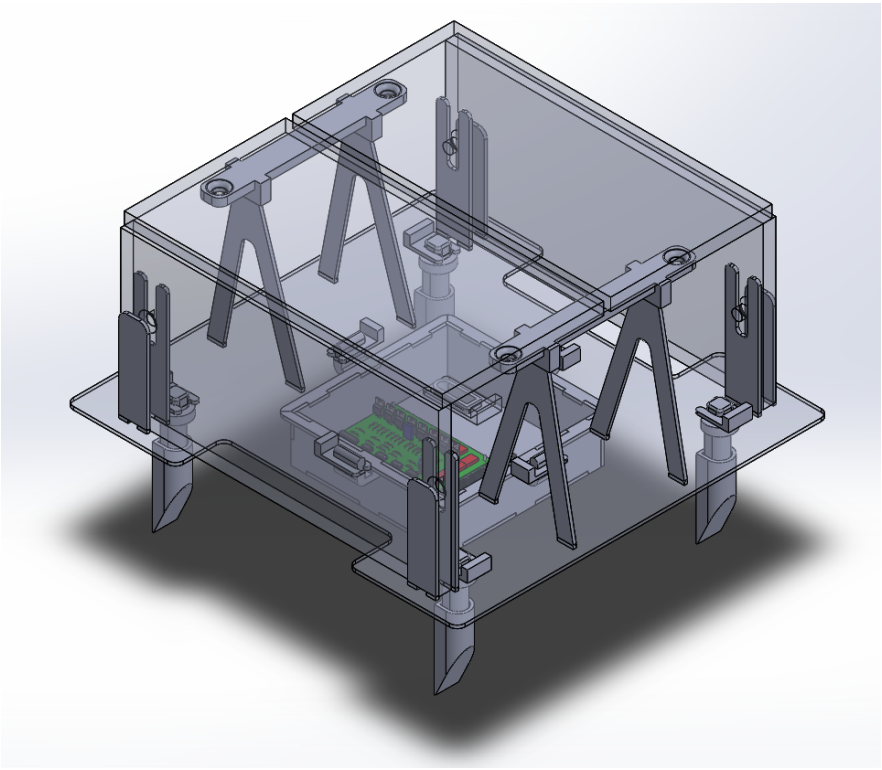

Figure 3.23: CAD model of the experiment setup.

2020 during the COVID-2019 outbreak which made it impossible to have access to Universidad UPB and a secondary location had to be chosen. The location selected was an available rooftop in the city of Envigado. For this reason the climate variables evaluated in section 4.4 only considers the data acquired from the meteorological station of Llanogrande.

Two experimental units were built, Figure 3.24 presents both units in their respective locations. This setup was designed to acquire data from three different orientations, for this specific case east, west and horizontal. In total eight flat modules were randomly picked from the University's existing stock and used for the experiments. As previously mentioned, each module consists of two SunPower C60 solar cells connected in series, each with a rated power of 3.42W.

For a month (Sep/25/2020 to Oct/23/2020) one of the sets was positioned at each location. The solar modules' position in the assembly was also rotated weekly, this way, by the end of the month each module had been facing every orientation. This strategy was used to minimize any possible bias caused by manufacturing differences between the modules.

A plastic cover was placed beneath both modules to minimize the effects of the albedo generated by the mounting surfaces. The final setups are shown in Figure 3.25. For both experiments the time interval between measurements was set to one minute and the device was restricted to send information only between 5am and 7pm, as the night hours represent no useful data for this study.

(a) Llanogrande's experiment.

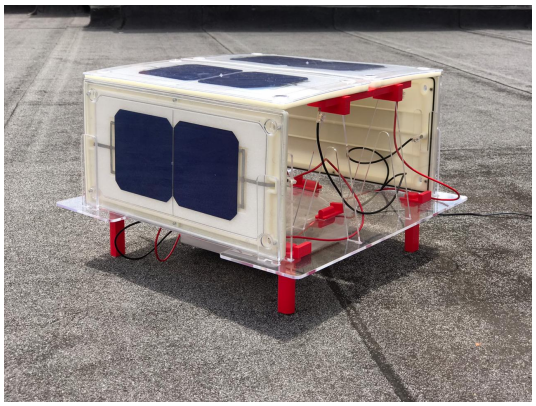

(b) Envigado's experiment.

Figure 3.24: Experimental setups on both locations.

Once per week, when the rotation of the modules was performed, a multimeter was used to ensure that the devices were still calibrated.

(a) Llanogrande's experiment final setup.

(b) Llanogrande's experiment final setup.

Figure 3.25: Experiments final setup.

Chapter 4

Results and analysis

This section presents the results of the experiments and contrasts them with the existing literature.

4.1 Raw results and data manipulation

Two of the 29 days evaluated (October 9th and 10th) were discarded due to communication problems with the IoT platform. A total of 21010 and 21070 data measurements were evaluated for Llanogrande and Envigado respectively. Each measurement consists of a timestamp, voltage and current of each module. Figure 4.1 presents the raw Isc and Voc data acquired by the measuring equipment located in Llanogrande, note that Sub-Figure 4.1c presents the average results for both horizontal modules. For a better look and understanding of the data presented in these graphs Figure 4.2 presents a zoom on October 11 from the average of horizontal modules.

For both experiments the two horizontal modules' Voc and Isc were averaged to evaluate them as one. Three different analyses were made to the collected information:

- First, to calculate and evaluate the average instant power per square meter (W/m^2) available on each module.
- Second, to calculate and compare the the total daily energy generation per square meter (Wh/m^2) of each module.
- The last one consisted in using the meteorological data recollected to evaluate how the climatic variables affect the performance of the solar modules, where the power per square meter (W/m^2) was the variable used to find the correlations.

The idea to calculate and use both power and energy per unit area for the results' analyses is to implement a more standard way to show the results. The vast majority of articles and information

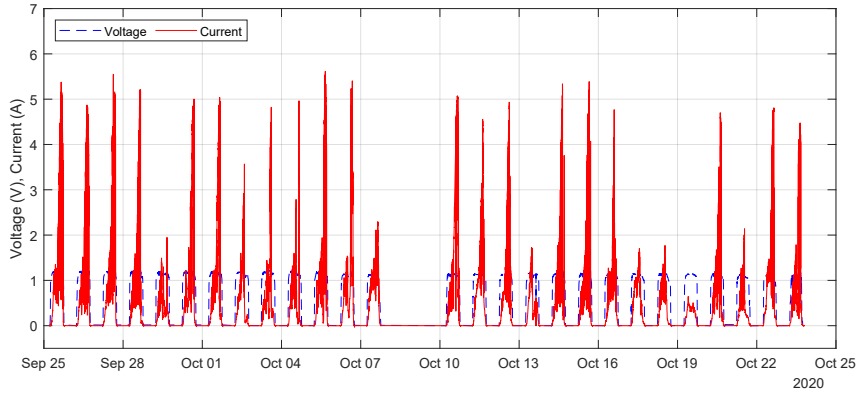

(a) West module current and voltage.

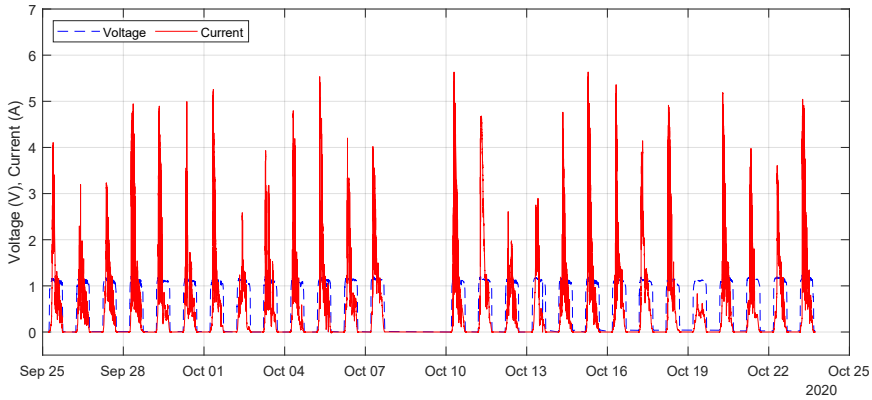

(b) East module current and voltage.

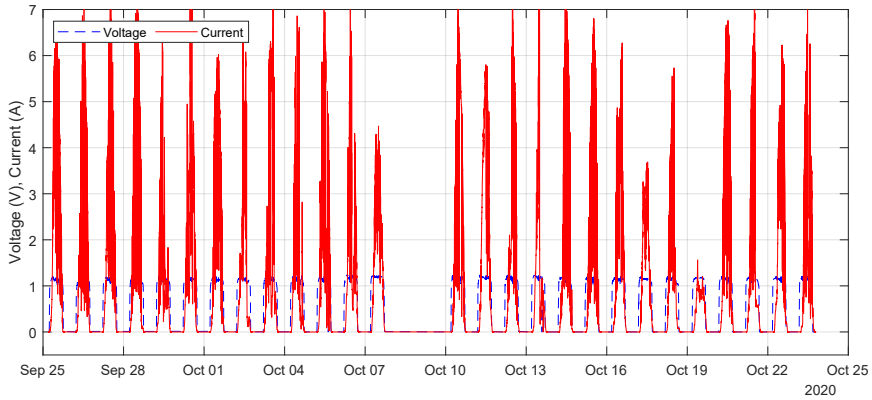

(c) Horizontal modules average current and voltage.

Figure 4.1: Voltage and current results for Llanogrande.

available related to PV technologies use these variables as they are easier to understand and compare.

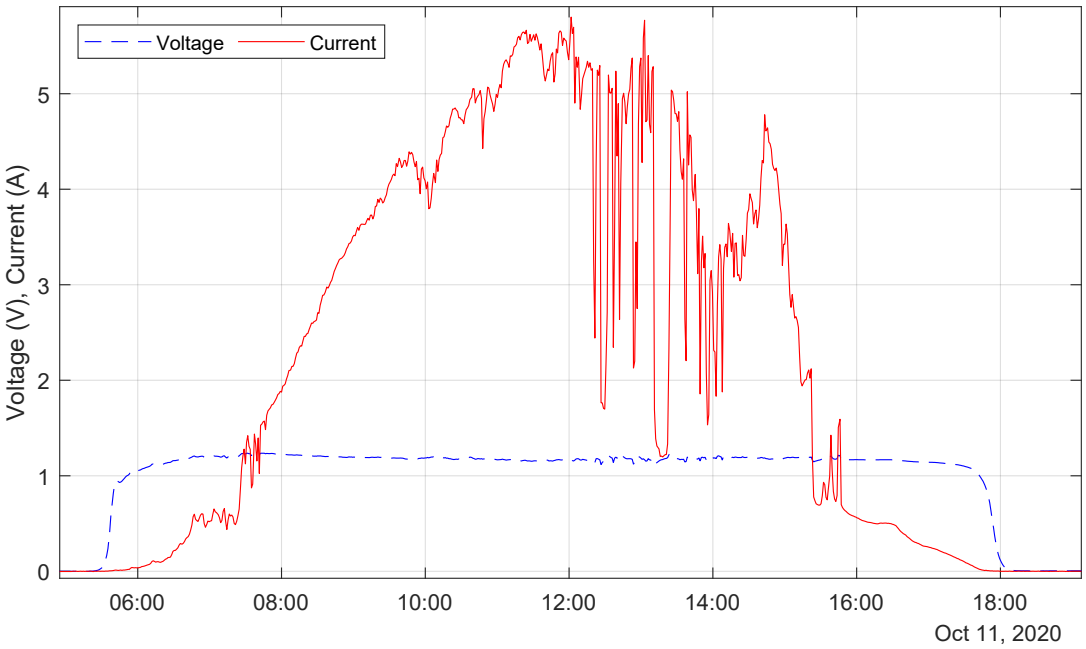

Figure 4.2: Llanogrande's horizontal voltage and current results for October 11.

The area of the cells used in the solar brick is $12.5cm\ x\ 12.5cm$, which for two cells per module equals $0.03125m^2$. This means all the results obtained for power and energy are divided by $0.03125m^2$ to get (W/m^2) and (Wh/m^2).

4.2 Power availability results

The first variable evaluated was power per area. The instant power of each module was calculated as the product between its Isc and Voc. Figure 4.3 shows the average instant available power per square meter for both locations and every orientation throughout the day.

Figure 4.3 shows that in both locations, as expected, the power available on the horizontal modules was higher than on each of the vertical ones. Table 4.1 presents the maximum power per orientation and its time stamp. It is important to notice that these power vs time curves also describe the behavior over time of the energy generation of the modules.

It is noticeable that Llanogrande's vertical maximum power is 8.47% and 29.37% higher than Envigado's for east and west respectively. The horizontal generation, on the other hand, was higher on Envigado by 0.85%. Both locations had their maximum power peaks at similar instances of the day, being the west oriented modules the most time diverging by only 20 minutes.

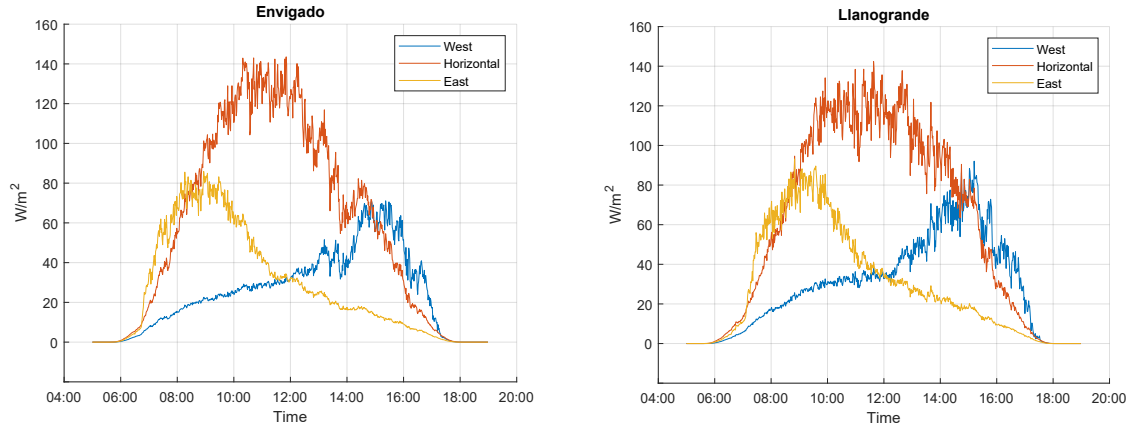

(a) Envigado's mean power.

(b) Llanogrande's mean power.

Figure 4.3: Mean instant power available per orientation.

Location	Orientation	Power (W/m^2)	Time
Envigado	East	85.9	8:56am
	West	71.16	2:52pm
	Horizontal	143.55	11:51am
Llanogrande	East	93.18	8:50am
	West	92.06	3:12pm
	Horizontal	142.34	11:38am

Table 4.1: Maximum instant power per orientation.

4.3 Energy generation results

To get an approximation of the energy generated by each cell the instant power (Isc x Voc) was integrated over time. Figure 4.4 presents the sum of energy generated by the modules during the 27 days of experiments.

The data sets were then divided by the area of the modules to get Wh/m^2 and grouped by days (energy generated per square meter per day). Before assessing the results a Normal Distribution test was done to the data sets in order to identify which statistical tests would be compatible for the analyses. The Anderson-Darling test was used and verified that all the data sets follow a normal distribution. Two-tailed t-tests were then used to analyze the results ($H_o : \mu_h = \mu_v$, $H_a : \mu_h \neq \mu_v$, $\alpha = .05$).

The daily average energy generation per square meter results for both locations and each orientation are shown in Figure 4.5. For this graph the daily generation data of each cell was used to create

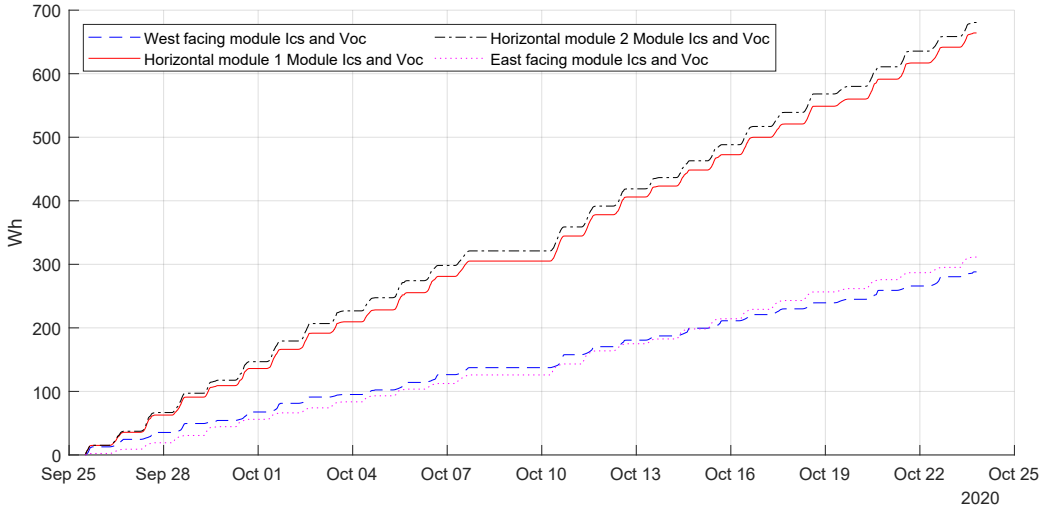

(a) Envigado's total energy generation.

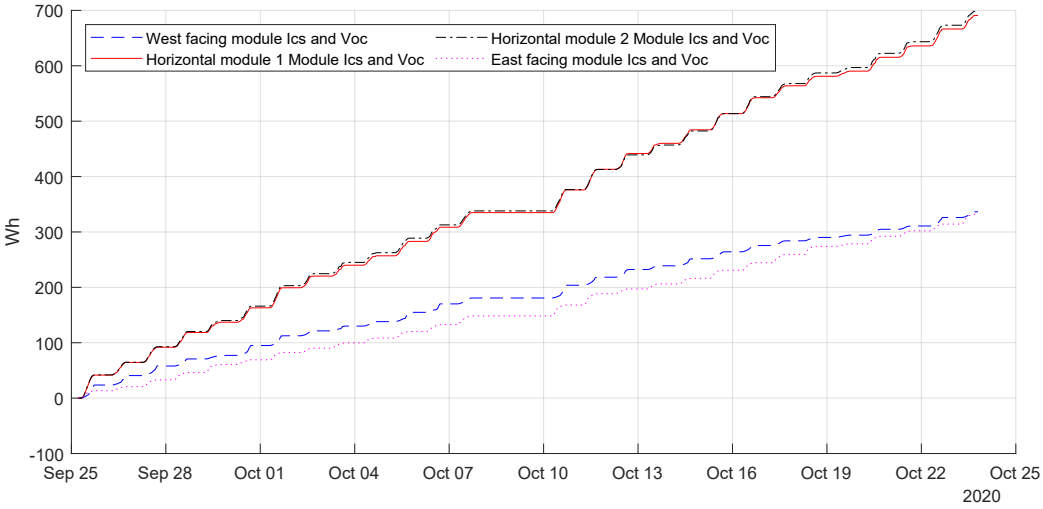

(b) Llanogrande's total energy generation.

Figure 4.4: Total energy generation per orientation.

violin plots to show both, the variance of data and its distribution. Here, a visual evidence of the normal distribution is presented.

Four t-tests were performed to evaluate if significant differences were found on the energy generation of the modules and locations.

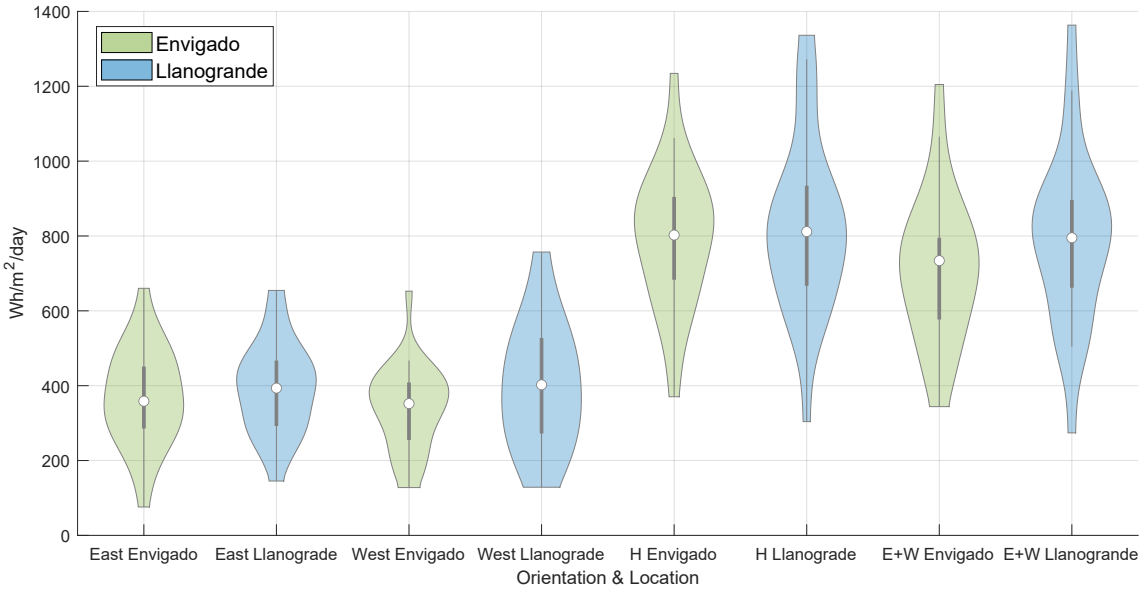

Figure 4.5: Comparison between locations (H: Horizontal, E: East, W: West).

4.3.1 T-test 1: East vs West on each location

The first analysis performed had as objective to compare the energy generated by both vertical modules on each location. Table 4.2 shows the results of the two-tailed t-test.

Location \ Orientation		East (n=27)	West (n=27)	*t-value*	*p*
Envigado	M	369.19	341.78	0.83	.41
	SD	128.68	113.43		
Llanogrande	M	393.67	398.76	-0.13	.89
	SD	119.87	163.27		

Table 4.2: t-test results for different vertical orientations on same locations.

As shown by the analysis, no significant difference was found between the vertical modules' energy generation on both locations (all p-values are higher than the alpha level used of 0.05). This result is in line with previous studies' findings (Hsieh et al., 2013; Brito et al., 2017; Díez-Mediavilla et al., 2019), where the east and west facades were found to be close to identical in energy generation.

4.3.2 T-test 2: (East + West) vs Horizontal on each location

For the next analysis the energy generated by both vertical modules was added and compared against the horizontal ones. Figure 4.6 and table 4.3 present the results.

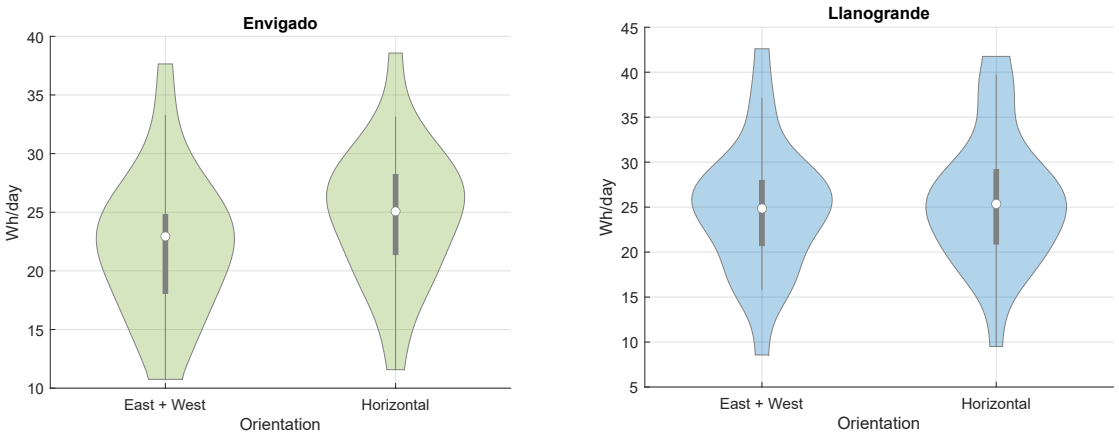

(a) Envigado's Vertical total vs horizontal.

(b) Llanogrande's Vertical total vs horizontal.

Figure 4.6: Vertical (East + West) vs horizontal results.

Location \ Orientation		Horizontal (n=27)	East + West (n=27)	*t-value*	*p*
Envigado	M	796.91	710.97	1.68	.09
	SD	184.95	189.94		
Llanogrande	M	823.29	792.43	0.49	.62
	SD	230.56	228.59		

Table 4.3: t-test results for horizontal vs total vertical on same locations.

For both locations there was no significant difference in the mean energy generated by the horizontal modules and the combination of the vertical ones. This result is similar to that of the studies performed in the northern temperate zone in the summer time as east and west orientations, individually, accounts for around 50% of the horizontal energy generation (Hsieh et al., 2013) or irradiance (Díez-Mediavilla et al., 2019). On the other hand, results differ from those of the studies performed during winter (Hsieh et al., 2013) as the solar position has significant changes for the northern temperate zone throughout the year. During winter at these regions, the horizontal generation drops in a higher proportion than the vertical, giving a higher advantage to east and west facades.

4.3.3 T-test 3: Location A vs Location B for each orientation

The third analysis focused on finding if there were any significant differences between the energy generation on each location for each orientation (table 4.4).

This analysis did not show a significant differences between the evaluated groups. This means that for the time frame in which the experiments were performed, the geographical locations had the same energy generation for each orientation.

Orientation \ Location		Envigado (n=27)	Llanogrande (n=27)	*t-value*	*p*
East	M	369.19	393.67	-0.72	.47
	SD	128.68	119.87		
West	M	341.78	398.76	-1.49	.14
	SD	113.43	163.28		
Horizontal	M	796.91	823.29	-0.46	.64
	SD	184.95	230.56		

Table 4.4: t-test results for same orientation in both locations.

4.3.4 T-test 4: Location A vs Location B (East + West + Horizontal)

The last analysis, shown in table 4.5 and Figure 4.7, considered the sum of the generation of the three orientations (East, West and Horizontal) in order to evaluate and compare the total energy generated in each location.

Orientation \ Location		Envigado (n=27)	Llanogrande (n=27)	*t-value*	*p*
Sum	M	1507.90	1615.7	-0.9714	.33
	SD	360.70	450.11		

Table 4.5: t-test results for the sum of all orientations.

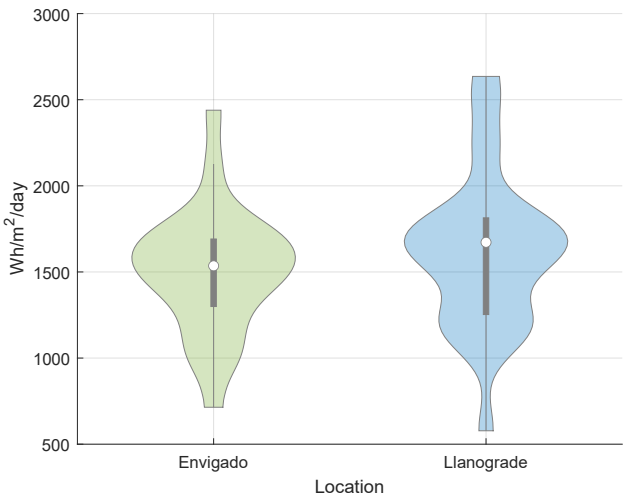

Figure 4.7: Comparison between both locations.

Again, this analysis didn't show either a significant difference between the evaluated groups, meaning that for the time frame in which the experiments were performed, the geographical locations had the same total energy generation.

4.4 Climatic variables

This section presents the evaluation of how the climatic variables were found to be related to the performance of BIPV in tropical regions. Irradiance, humidity and temperature are the variables to be evaluated in this section. As explained in section 3.4 only Llanogrande's experiment is going to be analyzed.

The meteorological station was configured to measure and send new data every 5 minutes. For this reason, it was necessary to readjust the data sets gathered from the experiment so that both data sets, from experiment and meteorological station, shared the same timestamps. It is also important to mention that the measurements made by the meteorological station and the experiment's device were not taken at the exact same time but in the same minute, meaning that there could be up to a 59 seconds difference between the timestamp of the measurements.

4.4.1 Irradiance

As stated in section 2.4, irradiance is the variable that most directly affects the performance of solar cells. It is important to note that the sensor used by the meteorological station measures horizontal direct radiation in W/m^2. Figure 4.8 presents the scatter plots of instant power generated by the modules vs irradiance.

From this initial evaluation it is clear that the two vertical orientations do not show a strong linear correlation with the irradiance. The east facing module was the vertical one with the best fit with an R^2 of only 0.36, meaning that its correlation coefficient equals 0.6, which is categorized as a moderate linear correlation (Ratner, 2009). On the other hand, the horizontal module had a strong linear correlation with an R^2 value of 0.82.

The lower R^2 values of the vertical modules can be interpreted as that for the same value of irradiance the modules obtained a wide range of possible power outputs. Taking into consideration that the irradiance measured by the meteorological stations corresponds to the direct horizontal radiation, the behavior of these curves could be explained by the fact that having high horizontal irradiance does not necessarily mean having high vertical irradiance, specially considering that the last one highly depends on the position of the sun, and thus on the time of the day (e.g. at 9am the sun does not directly irradiate west-facing surfaces, even if the horizontal irradiance at the time is high). In order to validate this hypothesis new evaluations were made where the data was segmented by hours. 9am, 12pm and 3pm were selected as the hours to be evaluated given that, as shown in section 4.2, the power peaks for the three orientations occur close to these time frames.

Figure 4.9 presents the scatter plots for measurements made from 9am to 9:59am. The figures shown in the left column correspond to the total points taken between this time frame. The data outside the 95% prediction interval were interpreted as outliers and removed from the analysis. The

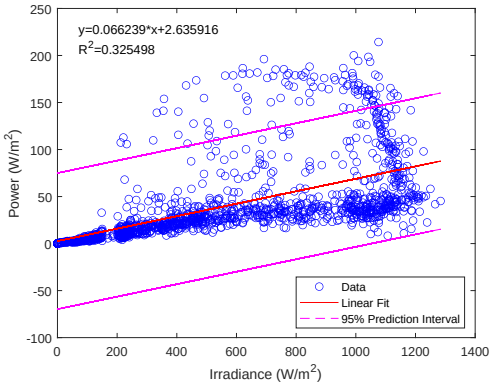

(a) West module power vs irradiance.

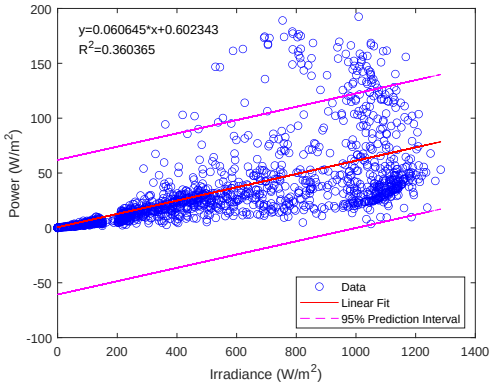

(b) East power vs irradiance.

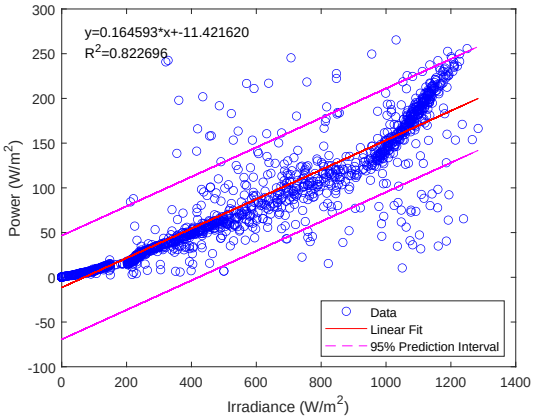

(c) Horizontal power vs irradiance.

Figure 4.8: Llanogrande's scatter plots of power vs irradiance.

figures in the right column show the new linear regressions and coefficient of determination (R^2) for each module.

From this analysis - made by taking only one hour of the day - it becomes clear that the horizontal module still presents the highest R^2 value with 0.88. However, both vertical modules had a significant increase in their R^2 value. In the initial analysis east module got 0.36, and increased to 0.79 on the analysis made for 9am. In the case of the west module, it started with 0.32 and got 0.55 on the new test. This large increase in the R^2 values shows that irradiance correlation with the power generated by the modules is dependent on the hour. This is specially true for the vertical modules.

The results for 9am, 12pm, 3pm and the entire day can be found on table 4.6.

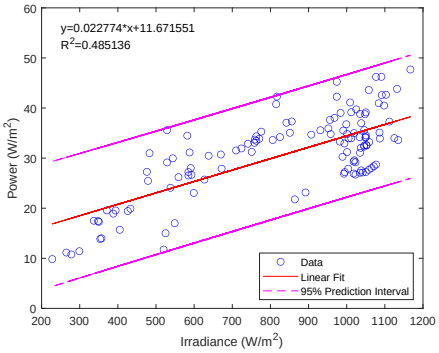

(a) West module power vs irradiance.

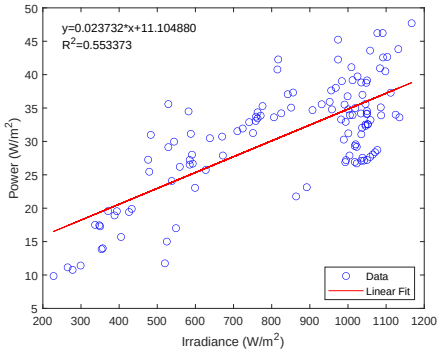

(b) West module power vs irradiance without outliers.

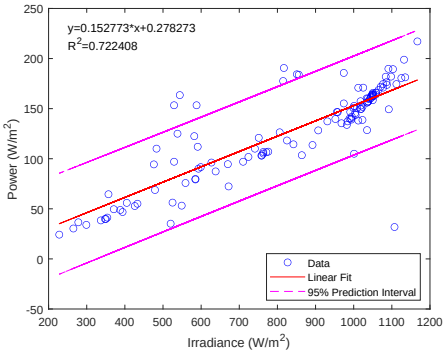

(c) Horizontal module power vs irradiance.

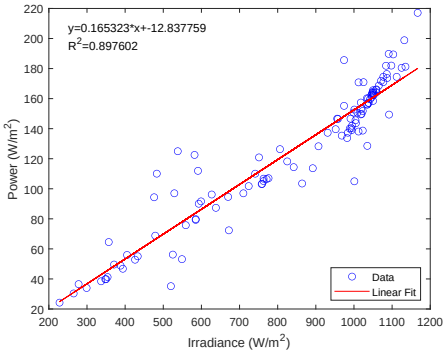

(d) Horizontal module power vs irradiance without outliers.

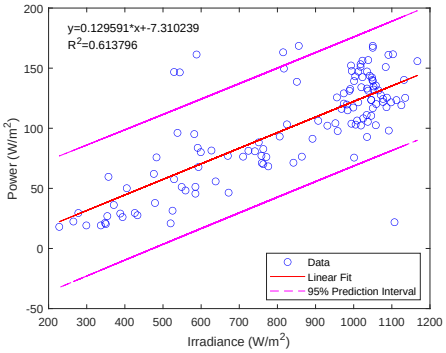

(e) East module power vs irradiance.

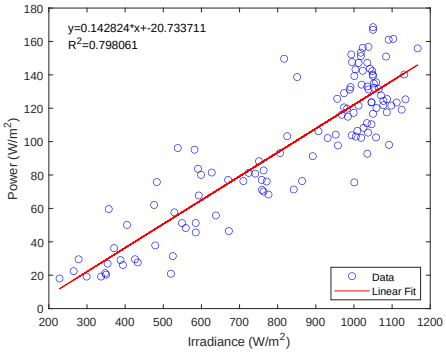

(f) East module power vs irradiance without outliers.

Figure 4.9: Llanogrande's scatter plots of power vs irradiance for 9 am measurements.

Power vs irradiation		All points	Without outliers	Amount of outliers
9am n=125	East	0.61	0.79	6
	West	0.49	0.55	1
	Horizontal	0.72	0.89	8
12pm n=160	East	0.61	0.7	5
	West	0.75	0.85	9
	Horizontal	0.81	0.94	8
3pm n=147	East	0.54	0.61	4
	West	0.8	0.9	9
	Horizontal	0.84	0.97	9
All day n=1419	East	0.36	0.49	83
	West	0.32	0.50	105
	Horizontal	0.82	0.94	82

Table 4.6: R^2 values for power vs irradiance.

4.4.2 Humidity

As with the irradiance, humidity's effect on the power was evaluated for each orientation. Figure 4.10 presents the total points obtained.

In the case of this analysis non of the modules power showed a strong correlation with humidity. However, all the plots suggest a negative relation, meaning that the higher the humidity is, the lower the power generated by the modules. To verify if the time of the day also had an effect on the correlation for the humidity, the same procedure made for irradiance was performed and the correlation was evaluated for 9am, 12pm and 3pm. Table 4.7 presents the results for the three analyzed hours.

After evaluating the results by hours it is clear that the effect of humidity in power was much lower in comparison with the irradiance.

In addition to this, the mean humidity per hour is shown in Figure 4.11. From this graph it is important to notice that humidity has the opposite behavior of irradiance, which has its peak at 12pm. Humidity, on the other hand, shows peaks at 8am and 6pm and a minimum at 12pm.

4.4.3 Temperature

Similarly as observed with irradiance and humidity, the effect of temperature on the power was evaluated for each orientation. Figure 4.12 presents the total points obtained. To verify if the time of the day also had an effect on the correlation for the temperature, the same procedure made for irradiance and humidity was performed and the correlation was evaluated for 9am, 12pm and 3pm. Table 4.8 presents the results for the three analyzed hours.

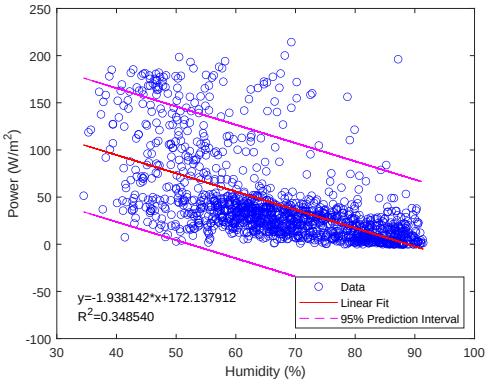

(a) West module power vs humidity.

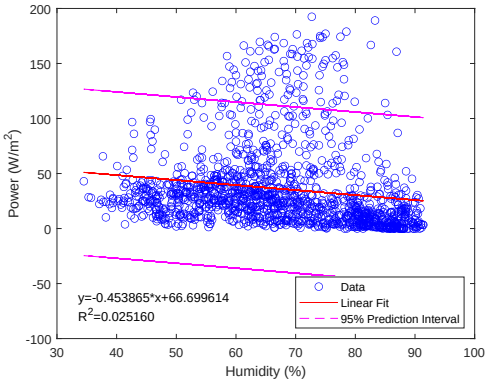

(b) East power vs humidity.

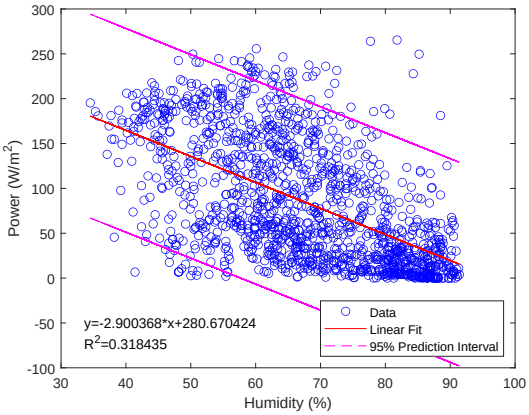

(c) Horizontal power vs humidity.

Figure 4.10: Llanogrande's scatter plots of power vs humidity.

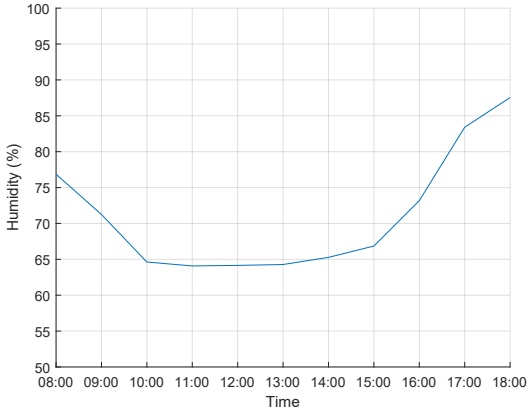

Figure 4.11: Llanogrande's mean humidity per hour.

Power vs humidity		All points	Without outliers	Amount of outliers
9am n=126	East	0.28	0.33	2
	West	0.13	0.19	5
	Horizontal	0.34	0.45	5
12pm n=161	East	0.25	0.43	6
	West	0.36	0.44	4
	Horizontal	0.36	0.52	7
3pm n=150	East	0.15	0.2	6
	West	0.34	0.46	4
	Horizontal	0.31	0.46	9
All day n=1416	East	0.03	0.09	100
	West	0.35	0.42	94
	Horizontal	0.32	0.41	67

Table 4.7: R^2 values for power vs humidity.

Power vs temperature		All points	Without outliers	Amount of outliers
9am n=125	East	0.39	0.47	3
	West	0.14	0.19	5
	Horizontal	0.42	0.54	6
12pm n=166	East	0.49	0.65	6
	West	0.49	0.63	6
	Horizontal	0.53	0.68	9
3pm n=150	East	0.24	0.32	5
	West	0.40	0.49	4
	Horizontal	0.38	0.51	8
All day n=1437	East	0.05	0.16	102
	West	0.38	0.49	96
	Horizontal	0.43	0.51	62

Table 4.8: R^2 values for power vs temperature.

For the case of temperature it is noticeable that the correlation found is the opposite to previous studies which reported a negative correlation. The reason for this behavior could be explained by the fact that those researches made the evaluations by isolating temperature, meaning that the rest of the variables stay fixed while temperature is changed. In this study, all variables had a combined influence as the experiments where performed under real operating conditions, and none of the variables was controlled. As seen in Figure 4.13 the mean temperature per hour was found to have the same behavior

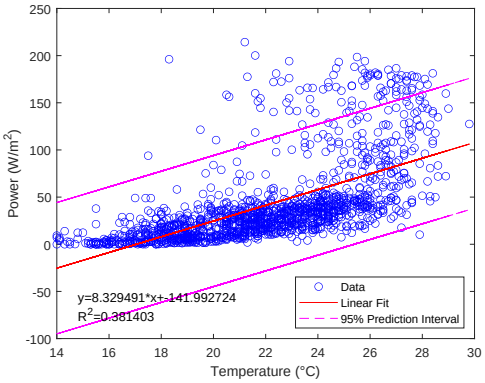

(a) West module power vs temperature.

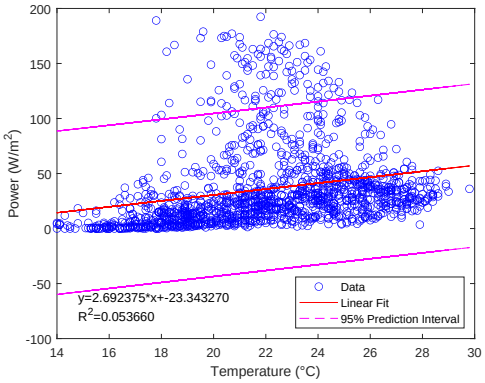

(b) East power vs temperature.

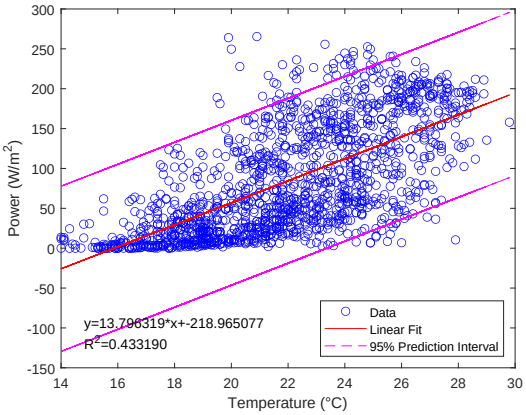

(c) Horizontal power vs temperature.

Figure 4.12: Llanogrande's scatter plots of power vs temperature.

as irradiance (bell-shape curve), for this reason, and as irradiance has the highest influence on the power generation, the negative effect of temperature was overcame by the positive effect of irradiance.

4.4.4 Combination of variables

Since the study was performed under real conditions the following approach was implemented to obtain an analytic equation capable of getting a good estimate of the power taking into consideration the three variables (irradiance, humidity and temperature), with the objective of obtaining a higher correlation value in comparison to those obtained in the previous sections. To do so, the power output of the cell was analyzed as a function of the irradiance, humidity and temperature $P = f(i, h, t)$, and the following equations were considered for the analysis:

1. $P = a * i + b * h + c * t$

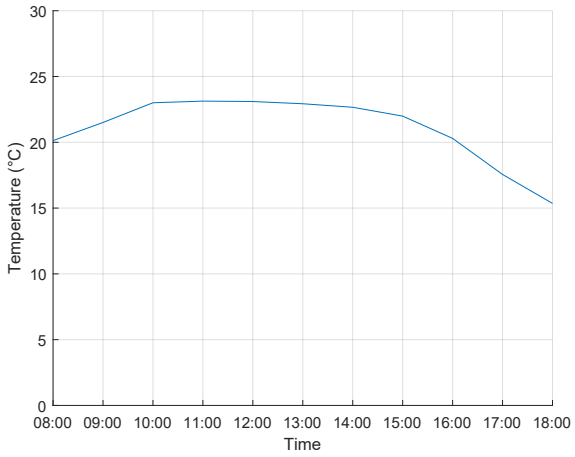

Figure 4.13: Llanogrande's mean temperature per hour.

2. $P = a * i + b * h^2 + c * t$

3. $P = a * i + b * h + c * t^2$

4. $P = (a * i + b * h)/(c * t)$

5. $P = (a * i + c * t)/(b * h)$

Variables i, h and t represent the irradiance, humidity and temperature respectively; whereas the coefficients a, b and c are constants to be found. An algorithm was written to find the coefficients a, b and c and also to identify which of the equations better describes the behavior of the modules. While-loops where used to iteratively test possible combinations of constants for each equation while maximizing the value of R^2.

The data used for this analysis was the same used for the complete day analyses from the previous chapters 4.4.1, 4.4.2 and 4.4.3. The constants a,b and c were initially evaluated from -100 to 100, with steps of 5. However, after getting the first results (which where between -15 and 10) the range was reduced from -20 to 20 with steps of 0.5.

The equation with the best fit was equation 1 ($P = a * i + b * h + c * t$), the coefficients and final equations obtained for each orientation are listed in Table 4.9.

Equation	Orientation
P = 0.5*i + 0.5*h + 2*t	Horizontal
P = 0.5*i + 3.5*h - 10*t	East
P = 0.5*i - 1.0*h + 4*t	West

Table 4.9: Equations for each orientation

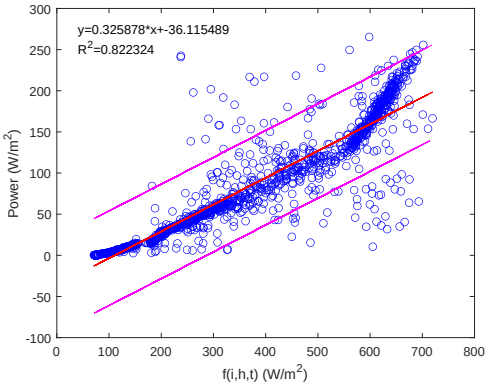

(a) Horizontal module's equation fit with outliers.

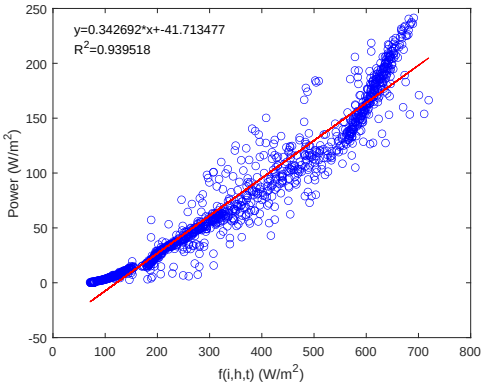

(b) Horizontal module's equation fit without outliers.

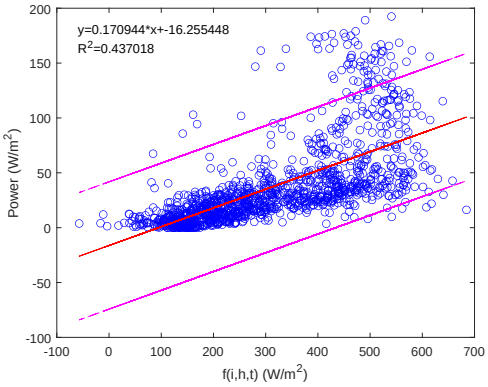

(c) East module's equation fit with outliers.

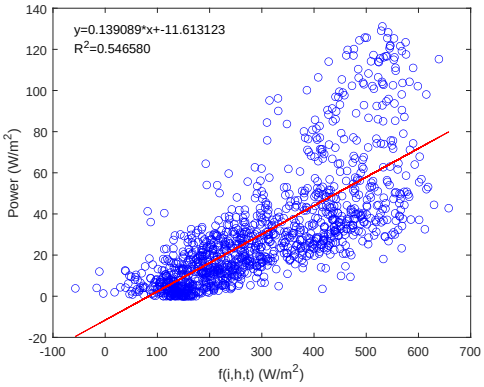

(d) East module's equation fit without outliers.

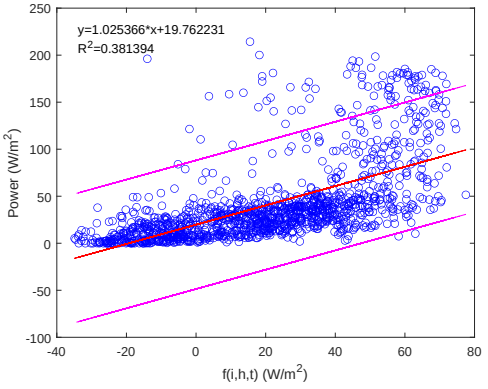

(e) West module's equation fit with outliers.

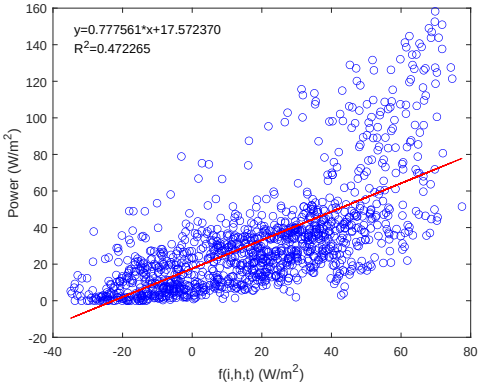

(f) West module's equation fit without outliers.

Figure 4.14: $P = a * i + b * h + c * t$ vs power scatter plot.

From the obtained results it is evident how for the vertical modules the R^2 values improve in comparison to those obtained by using only irradiance, humidity or temperature. The horizontal module, on the other hand, had close to equal results when only irradiance was used and when the three variables were combined. The final R^2 results of the different analyses before and after deleting outliers is shown in Tables 4.10 and 4.11.

R^2 values before deleting outliers				
Orientation	Individual			Combined
	Irradiance	Humidity	Temperature	
Horizontal	0.82	0.32	0.43	0.82
East	0.36	0.03	0.05	0.43
West	0.33	0.35	0.38	0.38

Table 4.10: R^2 with outliers

R^2 values after deleting outliers				
Orientation	Individual			Combined
	Irradiance	Humidity	Temperature	
Horizontal	0.94	0.41	0.51	0.94
East	0.49	0.09	0.16	0.55
West	0.50	0.42	0.49	0.47

Table 4.11: R^2 with outliers

Chapter 5

Conclusions and Future Work

5.1 Conclusions

The results gathered by the experiments carried out in this study helped identifying characteristics of the performance of BIPV technologies when located at tropical regions. Electrical and meteorological variables were used to evaluate the viability of the implementation of vertical BIPV and how the weather is able to affect its performance. The experiments were executed at Envigado and Llanogrande, both located in Colombia.

The results from both experiments showed that vertical BIPV oriented to east and west generate half of the energy of one that is in a horizontal position. This means that vertical BIPV oriented in these positions would only need twice the space to equal the generation of horizontal ones. This results make the potential of vertical PV technologies evident as urban areas count with extensive free vertical surfaces.

Vertical modules showed a clear difference in the generation profile in comparison with the horizontal ones. As expected, the horizontal modules had their power peak around 12pm when the horizontal irradiation is at its maximum. In contrast, the vertical modules had their power peaks around 9am for the east-facing ones and around 3pm for the west-facing ones. The time at which the power peak happened for each orientation was close to equal for the two locations evaluated, being the west oriented modules the most time distant by only 20 minutes.

The results obtained for the vertical modules showed that, in the locations at which the experiments were carried out, it would be equal to position vertical BIPV modules facing east or west. Horizontal modules also showed no significant differences between locations. Both locations used where found to be energetically equal for PV generation.

The meteorological variables analyses showed that irradiance, humidity and temperature had a correlation with the power generated by the modules. In the case of irradiance, as expected, the results

show a positive correlation, meaning that the higher the irradiance, the higher the power generated. For humidity a negative correlation was found, meaning that the higher the humidity, the lower the power generated. Temperature was found to also have a positive correlation, opposite to what was found on the state of the art, behavior that was explained by the stronger correlation of power with irradiance, which overcame the negative effect of the temperature. For the three meteorological variables, the horizontal modules showed a stronger correlation than the vertical ones. Finally, the analysis made to evaluate the effects of the three combined variables on the power generation of the solar modules was able to find equations which describe the behavior of the modules with a higher R^2 values in comparison to the individual analyses.

This study showed evidence of how lab-based PV experimentation and research can differ from real life results. The best example was the contradiction found on the influence of temperature on the power generation,. For this reason, it is important to perform field tests on these topics as a complement to the purely lab-based studies, and thus gain more real and applicable knowledge that allow a proper development and optimization of PV technologies, especially BIPV.

With regards to the experimental set-ups, the implementation of IoT to the monitoring system showed great potential for the remote evaluation of BIPV systems as it is a great tool to gather information that can then be used to identify possible system optimizations.

5.2 Future work

Further research has to be made in order to confirm that the FF does stay equal for all the modules when they are under the same meteorological conditions.

To accomplish a better understanding and more generalized conclusions it is necessary to study BIPV in more locations and for a longer period of time, ideally an entire year should be evaluated to see how the behaviour of the solar modules changes through out the year. On addition, it would be suggested to have more control over the meteorological data acquisition by using a monitoring system integrated to the same circuit. This way the meteorological and electrical data would be measured at the exact same time, potentially increasing the accuracy of the correlations found.

More PV technologies such as polycrystalline and thin-film should also be tested to identify the modules that would be the best fit for BIPV in tropical regions. Furthermore, future experiments should consider using full size solar panels on actual buildings to make a more realistic evaluation of these technologies.

Finally, technical and economical analyses and research should be carried out in order to have a complete understanding of the real viability of BIPV technologies, taking into consideration more aspects besides the energy generation.

Bibliography

Abel, D., Holloway, T., Harkey, M., Rrushaj, A., Brinkman, G., Duran, P., Janssen, M., and Denholm, P. (2018). Potential air quality benefits from increased solar photovoltaic electricity generation in the Eastern United States. *Atmospheric Environment*, 175(August 2017):65–74.

Acolgen (2020). Asociación colombiana de generadores de energía eléctrica.

Agrawal, B. and Tiwari, G. N. (2011). An energy and exergy analysis of building integrated photovoltaic thermal systems. *Energy Sources, Part A: Recovery, Utilization and Environmental Effects*, 33(7):649–664.

Ahmed, Y. (2020). Solar cell temperature and efficiency.

Ali, M. and Al-Kodmany, K. (2012). Tall buildings and urban habitat of the 21st century: A global perspective. *Buildings*, 2.

Allan, G., Eromenko, I., Gilmartin, M., Kockar, I., and McGregor, P. (2015). The economics of distributed energy generation: A literature review. *Renewable and Sustainable Energy Reviews*, 42:543–556.

Amprobe (2010). *SOLAR 600 Solar Analyzer*. Rev. D.

Andreani, L. C., Bozzola, A., Kowalczewski, P., Liscidini, M., and Redorici, L. (2019). Silicon solar cells: toward the efficiency limits. *Advances in Physics: X*, 4(1):1548305.

Andrews, R. W. and Pearce, J. M. (2013). The effect of spectral albedo on amorphous silicon and crystalline silicon solar photovoltaic device performance. *Solar Energy*, 91:233–241.

Arnoux, C. (2012). *FTV200SOLAR PANEL TESTERSI-V Tracer*. Rev. D.

Bayrak, F., Ertürk, G., and Oztop, H. F. (2017). Effects of partial shading on energy and exergy efficiencies for photovoltaic panels. *Journal of Cleaner Production*, 164:58–69.

Betancur, M., Camargo, V., Betancur, J., Velasquez-Lopez, A., Marulanda, J., and Toro, V. (2016). Recubrimiento con elementos optoelectrónicos. Colombia Patent, ref. 16064118.

BID, G. T. P. (2016). Smart grids colombia vision 2030 parte ii-mapa de ruta: Construcciòn y resultados (componente i).

Biyik, E., Araz, M., Hepbasli, A., Shahrestani, M., Yao, R., Shao, L., Essah, E., Oliveira, A. C., del Caño, T., Rico, E., Lechón, J. L., Andrade, L., Mendes, A., and Atli, Y. B. (2017). A key review of building integrated photovoltaic (BIPV) systems. *Engineering Science and Technology, an International Journal*, 20(3):833–858.

Böer, K. (1979). The physics of solar cells. *Journal of Applied Physics*, 50(8):5356–5370.

Bouraiou, A., Hamouda, M., Chaker, A., Mostefaoui, M., Lachtar, S., Sadok, M., Boutasseta, N., Othmani, M., and Issam, A. (2015). Analysis and evaluation of the impact of climatic conditions on the photovoltaic modules performance in the desert environment. *Energy Conversion and Management*, 106(October 2019):1345–1355.

BPSTATS (2019). BP Statistical Review of World Energy Statistical Review of World, 68th edition. *The Editor BP Statistical Review of World Energy*, pages 1–69.

Brennan, M. P., Abramase, A. L., Andrews, R. W., and Pearce, J. M. (2014). Erratum: Effects of spectral albedo on solar photovoltaic devices" (Solar Energy Materials and Solar Cells (2014) 124 (111-116)). *Solar Energy Materials and Solar Cells*, 125:297.

Brito, M. C., Freitas, S., Guimarães, S., Catita, C., and Redweik, P. (2017). The importance of facades for the solar PV potential of a Mediterranean city using LiDAR data. *Renewable Energy*, 111:85–94.

Carvajal-Romo, G., Valderrama-Mendoza, M., Rodríguez-Urrego, D., and Rodríguez-Urrego, L. (2019). Assessment of solar and wind energy potential in La Guajira, Colombia: Current status, and future prospects. *Sustainable Energy Technologies and Assessments*, 36(August):100531.

Catita, C., Redweik, P., Pereira, J., and Brito, M. C. (2014). Extending solar potential analysis in buildings to vertical facades. *Computers and Geosciences*, 66:1–12.

C.B.Honsberg, S. (2019). Photovoltaics education website.

Chakraborty, S. S., Kumar, R., Haldkar, A. K., and Ranjan, S. (2017). Mathematical method to find best suited PV technology for different climatic zones of India. *International Journal of Energy and Environmental Engineering*, 8(2):153–166.

Chander, S., Purohit, A., Sharma, A., Arvind, Nehra, S. P., and Dhaka, M. S. (2015). A study on photovoltaic parameters of mono-crystalline silicon solar cell with cell temperature.

Chen, F. and Yin, H. (2016). Fabrication and laboratory-based performance testing of a building-integrated photovoltaic-thermal roofing panel. *Applied Energy*, 177:271–284.

Cheng, L., Zhang, F., Li, S., Mao, J., Xu, H., Ju, W., Liu, X., Wu, J., Min, K., Zhang, X., and Li, M. (2020). Solar energy potential of urban buildings in 10 cities of China. *Energy*, 196.

Chitturi, S. R. P., Sharma, E., and Elmenreich, W. (2018). Efficiency of photovoltaic systems in mountainous areas. *2018 IEEE International Energy Conference, ENERGYCON 2018*, pages 1–6.

Chudinzow, D., Nagel, S., Güsewell, J., and Eltrop, L. (2020). Vertical bifacial photovoltaics - A complementary technology for the European electricity supply? *Applied Energy*, 264(December 2019):114782.

Chudinzow, D., Nagel, S., Güsewell, J., Eltrop, L., Guo, S., Walsh, T. M., Peters, M., Díez-Mediavilla, M., Rodríguez-Amigo, M. C., Dieste-Velasco, M. I., García-Calderón, T., Alonso-Tristán, C., Ghazali, A., Salleh, E. I., Haw, L. C., Mat, S., and Sopian, K. (2017). Performance and financial evaluation of various photovoltaic vertical facades on high-rise building in Malaysia. *Energy and Buildings*, 134(December 2019):306–318.

Corporation, S. (2014). *Solmetric PVA Brochure*. Rev. D.

Corporation, S. (2018). *Solmetric PVA-1500 Brochure*. Rev. D.

Cronemberger, J., Caamaño-Martín, E., and Sánchez, S. V. (2012). Assessing the solar irradiation potential for solar photovoltaic applications in buildings at low latitudes - Making the case for Brazil. *Energy and Buildings*, 55:264–272.

Cuce, E., Cuce, P. M., and Bali, T. (2013). An experimental analysis of illumination intensity and temperature dependency of photovoltaic cell parameters. *Applied Energy*, 111:374–382.

Dabou, R., Bouchafaa, F., Arab, A. H., Bouraiou, A., Draou, M. D., Neçaibia, A., and Mostefaoui, M. (2016). Monitoring and performance analysis of grid connected photovoltaic under different climatic conditions in south Algeria. *Energy Conversion and Management*, 130(December):200–206.

Dennis, K., Colburn, K., and Lazar, J. (2016). Environmentally beneficial electrification: The dawn of emissions efficiency'. *Electricity Journal*, 29(6):52–58.

Despotovic, M. and Nedic, V. (2015). Comparison of optimum tilt angles of solar collectors determined at yearly, seasonal and monthly levels. *Energy Conversion and Management*, 97:121–131.

Desthieux, G., Carneiro, C., Camponovo, R., Ineichen, P., Morello, E., Boulmier, A., Abdennadher, N., Dervey, S., and Ellert, C. (2018). Solar energy potential assessment on rooftops and facades in large built environments based on lidar data, image processing, and cloud computing. methodological background, application, and validation in geneva (solar cadaster). *Frontiers in Built Environment*, 4:14.

Diazgranados-Garzón, J. D., Romero-Bravo, J. C., Navarro-Estrada, L. I., Castillo-Sierra, R. D. J., Soto-Ortiz, J. D., and Pardo Gonzalez, M. (2019). Analysis of the Soiling Effect on Solar-Panel Power Efficiency in the Colombian Caribbean Region. *Revista Facultad de Ingeniería Universidad de Antioquia*.

Díez-Mediavilla, M., Rodríguez-Amigo, M. C., Dieste-Velasco, M. I., García-Calderón, T., and Alonso-Tristán, C. (2019). The PV potential of vertical façades: A classic approach using experimental data from Burgos, Spain. *Solar Energy*, 177(October 2018):192–199.

Dittrich, T. (2018). Basic Characteristics and Characterization of Solar Cells. *Materials Concepts for Solar Cells*, pages 3–43.

DNVGL (2017). DNV GL ENERGY TRANSITION Outlook - Key charts.

DNVGL (2017a). Executive Summary.

DNVGL (2017b). Maritime forecast to 2050: Energy transition outlook 2017. *DNV GL, Høvik, Norway*.

DNVGL (2017). Renewables, Power and Energy Use. Forecast 2050.

Doljak, D. L., Stanojević, G. B., Radovanović, M. M., and Malinović-Milicević, S. B. (2018). Estimation of photovoltaic power generation potential in Serbia based on irradiance, air temperature, and wind speed data. *Thermal Science*, 2018(6):2297–2307.

Drif, M., Mellit, A., Aguilera, J., and Pérez, P. J. (2012). A comprehensive method for estimating energy losses due to shading of GC-BIPV systems using monitoring data. *Solar Energy*, 86(9):2397–2404.

Dubey, S., Sarvaiya, J. N., and Seshadri, B. (2013). Temperature dependent photovoltaic (PV) efficiency and its effect on PV production in the world - A review. *Energy Procedia*, 33:311–321.

Durán, E., Andújar, J. M., Enrique, J. M., and Pérez-Oria, J. M. (2012). Determination of PV generator I-V/P-V characteristic curves using a DC-DC converter controlled by a virtual instrument. *International Journal of Photoenergy*, 2012.

Durán, E., Galán, J., Andújar, J. M., and Sidrach-de Cardona, M. (2008). A new method to obtain I-V characteristics curves of photovoltaic modules based on SEPIC and cuk converters. *EPE Journal (European Power Electronics and Drives Journal)*, 18(2):5–15.

Duran, E., Piliougine, M., Sidrach-De-Cardona, M., Galan, J., and Andujar, J. M. (2008). Different methods to obtain the I-V curve of PV modules: A review. *Conference Record of the IEEE Photovoltaic Specialists Conference*.

Electronic, S. (2018). *PV210 Solar PV tester and I-V curve tracer*. Rev. D.

Elsayed, M. S. (2016). Optimizing thermal performance of building-integrated photovoltaics for upgrading informal urbanization. *Energy and Buildings*, 116:232–248.

EnergíaEstratégica (2020). Â¿Cómo se prepara el sistema eléctrico colombiano? XM revela cómo integrará 2.000 MW eólicos y solares.

Erkaya, Y., Flory, I., and Marsillac, S. X. (2014). Development of a string level I-V curve tracer. *2014 IEEE 40th Photovoltaic Specialist Conference, PVSC 2014*, pages 3104–3107.

Eslava R., J. A. (1993). Climatología y diversidad climática de Colombia.

Fouad, M. M., Shihata, L. A., and Morgan, E. S. I. (2017). An integrated review of factors influencing the performance of photovoltaic panels. *Renewable and Sustainable Energy Reviews*, 80(July 2016):1499–1511.

Gharakhani Siraki, A. and Pillay, P. (2012). Study of optimum tilt angles for solar panels in different latitudes for urban applications. *Solar Energy*, 86(6):1920–1928.

Ghazali, A., Salleh, E. I., Haw, L. C., Mat, S., and Sopian, K. (2017). Performance and financial evaluation of various photovoltaic vertical facades on high-rise building in Malaysia. *Energy and Buildings*, 134:306–318.

Giraldo-Pérez, J. P., Orrego-García, J. S., Ospina-Metaute, C. C., and Velásquez-López, A. (2020). Simplified method to compare the performance of a solar cell under different optical conditions and orientations. In Figueroa-García, J. C., Garay-Rairán, F. S., Hernández-Pérez, G. J., and Díaz-Gutierrez, Y., editors, *Applied Computer Sciences in Engineering*, pages 477–488, Cham. Springer International Publishing.

Green, M. A. (1981). Solar cell fill factors: General graph and empirical expressions. *Solid State Electronics*, 24(8):788–789.

Groppi, D., de Santoli, L., Cumo, F., and Astiaso Garcia, D. (2018). *A GIS-based model to assess buildings energy consumption and usable solar energy potential in urban areas*, volume 40. Elsevier B.V.

Guerriero, P., Cennamo, P. A., and Daliento, S. (2018). A portable circuit for real time curve tracing for solar panels embedded in solar fields. *SPEEDAM 2018 - Proceedings: International Symposium on Power Electronics, Electrical Drives, Automation and Motion*, pages 829–834.

Gul, M., Kotak, Y., Muneer, T., and Ivanova, S. (2018). Enhancement of albedo for solar energy gain with particular emphasis on overcast skies. *Energies*, 11(11):1–18.

Guo, S., Walsh, T. M., and Peters, M. (2013). Vertically mounted bifacial photovoltaic modules: A global analysis. *Energy*, 61:447–454.

Gwandu, B. and Creasey, D. (1995). Humidity: a factor in the appropriate positioning of a photovoltaic power station. *Renewable Energy*, 6(3):313–316.

Hecktheuer, L. A., Krenzinger, A., and Prieb, C. W. M. (2002). Methodology for Photovoltaic Modules Characterization and Shading Effects Analysis. *Journal of the Brazilian Society of Mechanical Sciences*, 24:26 – 32.

Hertwich, E. G., Gibon, T., Bouman, E. A., Arvesen, A., Suh, S., Heath, G. A., Bergesen, J. D., Ramirez, A., Vega, M. I., and Shi, L. (2015). Integrated life-cycle assessment of electricity-supply scenarios confirms global environmental benefit of low-carbon technologies. *Proceedings of the National Academy of Sciences of the United States of America*, 112(20):6277–6282.

Holmgren, W. F., Hansen, C. W., and Mikofski, M. A. (2018). pvlib python: a python package for modeling solar energy systems. *Journal of Open Source Software*, 3(29):884.

Horváth, I. (2008). Differences between 'research in design context' and 'design inclusive research' in the domain of industrial design engineering. *Journal of Design Research*, 7(1):61–83.

Horváth, I. et al. (2007). Comparison of three methodological approaches of design research. In *DS 42: Proceedings of ICED 2007, the 16th International Conference on Engineering Design, Paris, France, 28.-31.07. 2007*, pages 361–362.

Hsieh, C. M., Chen, Y. A., Tan, H., and Lo, P. F. (2013). Potential for installing photovoltaic systems on vertical and horizontal building surfaces in urban areas. *Solar Energy*, 93:312–321.

Huld, T. and Gracia Amillo, A. M. (2015). Estimating PV module performance over large geographical regions: The role of irradiance, air temperature, wind speed and solar spectrum. *Energies*, 8(6):5159–5181.

Hwang, T., Kang, S., and Kim, J. T. (2012). Optimization of the building integrated photovoltaic system in office buildings - Focus on the orientation, inclined angle and installed area. In *Energy and Buildings*, volume 46, pages 92–104.

IEA (2019). Global energy & co2 status report 2019.

Ineichen, P. and Perez, R. (2002). A new airmass independent formulation for the linke turbidity coefficient. *Solar Energy*, 73(3):151–157.

Instruments, H. (2019). *I-V500wRel. 1.01â€“06/03/19I-V curve tracer and IVCK tester up to 15A or 1500VDC*. Rev. D.

Izquierdo, S., Rodrigues, M., and Fueyo, N. (2008). A method for estimating the geographical distribution of the available roof surface area for large-scale photovoltaic energy-potential evaluations. *Solar Energy*, 82(10):929–939.

Jacobs, S. B. (2017). The energy prosumer.

Jakubiec, J. A. and Reinhart, C. F. (2013). A method for predicting city-wide electricity gains from photovoltaic panels based on lidar and gis data combined with hourly daysim simulations. *Solar Energy*, 93:127–143.

Jaugsch, F. and Löwner, M. O. (2016). Estimation of solar energy on vertical 3D building walls on city quarter scale. *International Archives of the Photogrammetry, Remote Sensing and Spatial Information Sciences - ISPRS Archives*, 42(2W2):135–143.

Jelle, B. P. (2016). Building integrated photovoltaics: A concise description of the current state of the art and possible research pathways. *Energies*, 9(1):1–30.

Jiménez, M. J., Madsen, H., Bloem, J. J., and Dammann, B. (2008). Estimation of non-linear continuous time models for the heat exchange dynamics of building integrated photovoltaic modules. *Energy and Buildings*, 40(2):157–167.

Jordehi, A. R. (2016). Parameter estimation of solar photovoltaic (PV) cells: A review. *Renewable and Sustainable Energy Reviews*, 61:354–371.

Kalogirou, S. (2017). *McEvoy's handbook of photovoltaics: fundamentals and applications*. Academic Press.

Kämpf, J. H. and Robinson, D. (2009). A hybrid CMA-ES and HDE optimisation algorithm with application to solar energy potential. *Applied Soft Computing Journal*, 9(2):738–745.

Kawamura, H., Naka, K., Yonekura, N., Yamanaka, S., Kawamura, H., Ohno, H., and Naito, K. (2003). Simulation of I-V characteristics of a PV module with shaded PV cells. *Solar Energy Materials and Solar Cells*, 75(3-4):613–621.

Kaynak, S., Kaynak, B., and Özmen, A. (2018). A software tool development study for solar energy potential analysis. *Energy and Buildings*, 162:134–143.

Kempe, M. D. (2006). Modeling of rates of moisture ingress into photovoltaic modules. *Solar Energy Materials and Solar Cells*, 90(16):2720–2738.

Kumar, N. M., Navothna, B., and Minz, M. (2018). Performance comparison of building integrated multi-wattage photovoltaic generators mounted vertically and horizontally. *Proceedings of the 2017 International Conference On Smart Technology for Smart Nation, SmartTechCon 2017*, pages 69–74.

Kumar, N. M., Sudhakar, K., and Samykano, M. (2020). Performance evaluation of CdTe BIPV roof and façades in tropical weather conditions. *Energy Sources, Part A: Recovery, Utilization and Environmental Effects*, 42(9):1057–1071.

Lana S.PANTIC, T. M. P. and MiLOSAVLJEVIC, D. D. (2013). a Practical Field Study of Performances of Solar. *University of NiS, Faculty of Sciences and MAthematics, Department of Physic, Republic of Serbia*, page 16.

Laveyne, J. I., Bozalakov, D., Van Eetvelde, G., and Vandevelde, L. (2020). Impact of Solar Panel Orientation on the Integration of Solar Energy in Low-Voltage Distribution Grids. *International Journal of Photoenergy*, 2020.

Leilaeioun, M. and Holman, Z. C. (2016). Accuracy of expressions for the fill factor of a solar cell in terms of open-circuit voltage and ideality factor. *Journal of Applied Physics*, 120(12).

López, A. R., Krumm, A., Schattenhofer, L., Burandt, T., Montoya, F. C., Oberländer, N., and Oei, P. Y. (2020). Solar PV generation in Colombia - A qualitative and quantitative approach to analyze the potential of solar energy market. *Renewable Energy*, 148:1266–1279.

Lu, L. and Law, K. M. (2013). Overall energy performance of semi-transparent single-glazed photovoltaic (PV) window for a typical office in Hong Kong. *Renewable Energy*, 49:250–254.

Luna, J. G. P., Coria, L. A. M., Iniesta, S. A., Xochimitl, S. J., and González, A. E. J. (2014). Modulo trazador de curvas para caracterizar elementos o dispositivos en la gama de nanoamperes. In *SOMI Congreso de Instrumentación*.

Mahmoud, M. M. (2006). Transient analysis of a pv power generator charging a capacitor for measurement of the i–v characteristics. *Renewable Energy*, 31(13):2198–2206.

Mastekbayeva, G. A. and Kumar, S. (2000). Effect of dust on the transmittance of low density polyethylene glazing in a tropical climate. *Solar Energy*, 68(2):135–141.

McCartney, M. (2009). Living with dams: Managing the environmental impacts. *Water Policy*, 11(SUPPL. 1):121–139.

Mekhilef, S., Saidur, R., and Kamalisarvestani, M. (2012). Effect of dust, humidity and air velocity on efficiency of photovoltaic cells. *Renewable and Sustainable Energy Reviews*, 16(5):2920–2925.

Meral, M. E. and Diner, F. (2011). A review of the factors affecting operation and efficiency of photovoltaic based electricity generation systems. *Renewable and Sustainable Energy Reviews*, 15(5):2176–2184.

Moharram, K. A., Abd-Elhady, M. S., Kandil, H. A., and El-Sherif, H. (2013). Enhancing the performance of photovoltaic panels by water cooling. *Ain Shams Engineering Journal*, 4(4):869–877.

Mondol, J. D., Yohanis, Y. G., and Norton, B. (2007). The impact of array inclination and orientation on the performance of a grid-connected photovoltaic system. *Renewable Energy*, 32(1):118–140.

Nayak, P. K., Mahesh, S., Snaith, H. J., and Cahen, D. (2019). Photovoltaic solar cell technologies: analysing the state of the art. *Nature Reviews Materials*, 4(4):269.

NREL (2019a). Best research-cell efficiency chart.

NREL (2019b). Champion photovoltaic module efficiency chart.

(NREL), T. N. R. E. L. (2020a). National solar radiation database.

(NREL), T. N. R. E. L. (2020b). Sam libraries.

Ordenes, M., Marinoski, D. L., Braun, P., and Rüther, R. (2007). The impact of building-integrated photovoltaics on the energy demand of multi-family dwellings in Brazil. *Energy and Buildings*, 39(6):629–642.

Ospina-Metaute, C. C., Betancur, E., Medina-Garzón, L. F., Marulanda-Bernal, J. I., and Velásquez-López, A. (2020). Optimization of the orientation of vertical surfaces based on geographic parameters for solar energy harvesting. In Figueroa-García, J. C., Garay-Rairán, F. S., Hernández-Pérez, G. J., and Díaz-Gutierrez, Y., editors, *Applied Computer Sciences in Engineering*, pages 453–464, Cham. Springer International Publishing.

Owusu, P. A. and Asumadu-Sarkodie, S. (2016). A review of renewable energy sources, sustainability issues and climate change mitigation. *Cogent Engineering*, 3(1).

Peng, C., Huang, Y., and Wu, Z. (2011). Building-integrated photovoltaics (BIPV) in architectural design in China. *Energy and Buildings*, 43(12):3592–3598.

Pérez, G., Coma, J., Martorell, I., and Cabeza, L. F. (2014). Vertical Greenery Systems (VGS) for energy saving in buildings: A review. *Renewable and Sustainable Energy Reviews*, 39:139–165.

Pérez-Alonso, J., Pérez-García, M., Pasamontes-Romera, M., and Callejón-Ferre, A. J. (2012). Performance analysis and neural modelling of a greenhouse integrated photovoltaic system. *Renewable and Sustainable Energy Reviews*, 16(7):4675–4685.

Piliougine, M., Carretero, J., Mora-Lopez, L., and Sidrach-de Cardona, M. (2011). Experimental system for currentâ€“voltage curve measurement of photovoltaic modules under outdoor conditions. *Progress in Photovoltaics: Research and Applications*, 19(5):591–602.

Qu, H. and Li, X. (2019). Temperature dependency of the fill factor in PV modules between 6 and 40 °C. *Journal of Mechanical Science and Technology*, 33(4):1981–1986.

Quesada, G., Rousse, D., Dutil, Y., Badache, M., and Hallé, S. (2012). A comprehensive review of solar facades. opaque solar facades. *Renewable and Sustainable Energy Reviews*, 16(5):2820 – 2832.

Ramaprabha, R., Jubair, S. H., Suhas, K., and Lokesh, A. (2015). Design and implementation of efficient curve tracer for photovoltaic system under partial shaded conditions. *International Journal on Electrical Engineering and Informatics*, 7(1):140–149.

Ratner, B. (2009). The correlation coefficient: Its values range between 1/1, or do they. *Journal of Targeting, Measurement and Analysis for Marketing*, 17(2):139–142.

Redweik, P., Catita, C., and Brito, M. (2013). Solar energy potential on roofs and facades in an urban landscape. *Solar Energy*, 97:332–341.

Reischauer, I. W. and Rix, A. J. (2019). Design of a low cost multi-module capacitive IV curve tracer for PV module mismatch characterisation. *Proceedings - 2019 Southern African Universities Power Engineering Conference/Robotics and Mechatronics/Pattern Recognition Association of South Africa, SAUPEC/RobMech/PRASA 2019*, pages 340–346.

Reusch, M., Bivour, M., Hermle, M., and Glunz, S. W. (2013). Fill factor limitation of silicon heterojunction solar cells by junction recombination. *Energy Procedia*, 38:297–304.

Revesz, M., Oswald, S. M., Trimmel, H., Weihs, P., and Zamini, S. (2018a). Potential increase of solar irradiation and its influence on PV facades inside an urban canyon by increasing the ground-albedo. *Solar Energy*, 174(August):7–15.

Revesz, M., Oswald, S. M., Trimmel, H., Weihs, P., and Zamini, S. (2018b). Potential increase of solar irradiation and its influence on PV facades inside an urban canyon by increasing the ground-albedo. *Solar Energy*, 174(August):7–15.

Riley, C. and Tolbert, L. (2015). An online autonomous i–v tracer for pv monitoring applications. In *2015 IEEE Power & Energy Society General Meeting*, pages 1–5. IEEE.

Ritzen, M., Vroon, Z., Rovers, R., Geurts, C., and Blocken, B. (2015). Real Life Lab BIPV field testing in the Netherlands. *2015 IEEE 42nd Photovoltaic Specialist Conference, PVSC 2015*, pages 3–7.

Rivai, A. and Rahim, N. A. (2014). Binary-based tracer of photovoltaic array characteristics. *IET Renewable Power Generation*, 8(6):621–628.

Rodríguez-Urrego, D. and Rodríguez-Urrego, L. (2018). Photovoltaic energy in Colombia: Current status, inventory, policies and future prospects. *Renewable and Sustainable Energy Reviews*, 92(May 2017):160–170.

Rüther, R. and Braun, P. (2009). Energetic contribution potential of building-integrated photovoltaics on airports in warm climates. *Solar Energy*, 83(10):1923–1931.

Saidan, M., Albaali, A. G., Alasis, E., and Kaldellis, J. K. (2016). Experimental study on the effect of dust deposition on solar photovoltaic panels in desert environment. *Renewable Energy*, 92:499–505.

Santos, Í. P. D. and Rüther, R. (2012). The potential of building-integrated (BIPV) and building-applied photovoltaics (BAPV) in single-family, urban residences at low latitudes in Brazil. *Energy and Buildings*, 50:290–297.

Savvides, A., Vassiliades, C., Michael, A., and Kalogirou, S. (2019). Siting and building-massing considerations for the urban integration of active solar energy systems. *Renewable Energy*, 135(2019):963–974.

Seapan, M., Hishikawa, Y., Yoshita, M., and Okajima, K. (2020). Temperature and irradiance dependences of the current and voltage at maximum power of crystalline silicon PV devices. *Solar Energy*, 204(May):459–465.

Shahatha Salim, M., Mohammed Najim, J., Mohammed Salih, S., and Mohammed Salih, S. (2013). Practical Evaluation of Solar Irradiance Effect on PV Performance. *Energy Science and Technology*, 6(62):36–40.

Shahsavari, A. and Akbari, M. (2018). Potential of solar energy in developing countries for reducing energy-related emissions. *Renewable and Sustainable Energy Reviews*, 90(June 2017):275–291.

Shukla, A. K., Sudhakar, K., and Baredar, P. (2017). Recent advancement in bipv product technologies: A review. *Energy and Buildings*, 140:188–195.

Singh, R. (2009). Why silicon is and will remain the dominant photovoltaic material. *Journal of Nanophotonics*, 3(1):032503.

Soonmin, H., Lomi, A., Okoroigwe, E. C., and Urrego, L. R. (2019). Investigation of solar energy: The case study in Malaysia, Indonesia, Colombia and Nigeria. *International Journal of Renewable Energy Research*, 9(1):86–95.

Stephan, P. (2019). Development of instrumentation of solar bricks.

Tan, C. M., Chen, B. K. E., and Toh, K. P. (2010). Humidity study of a-Si PV cell. *Microelectronics Reliability*, 50(9-11):1871–1874.

Tian, W., Wang, Y., Ren, J., and Zhu, L. (2007). Effect of urban climate on building integrated photovoltaics performance. *Energy Conversion and Management*, 48(1):1–8.

Unidad de Planeación Minero Energética, Banco Interamericano de Desarrollo, Ministerio de Minas y Energía, and las Comunicaciones, M. d. T. d. l. I. y. (2016). Parte I Antecedentes y Marco Conceptual del Análisis, Evaluación y Recomendaciones para la Implementación de Redes Inteligentes en Colombia. *Smart Grids Colombia Vision 2030*, page 81.

Vargas Gil, G. M., Bittencourt Aguiar Cunha, R., Giuseppe Di Santo, S., Machado Monaro, R., Fragoso Costa, F., and Sguarezi Filho, A. J. (2020). Photovoltaic energy in South America: Current state and grid regulation for large-scale and distributed photovoltaic systems. *Renewable Energy*, 162:1307–1320.

Vats, K. and Tiwari, G. N. (2012). Performance evaluation of a building integrated semitransparent photovoltaic thermal system for roof and faade. *Energy and Buildings*, 45:211–218.

Velasquez-Lopez, A., Lopez, A., Ortiz, V., Gonzalez, J., Amaya, J., Marulanda, J., Munera, L., and Aguilar, J. (2014). Elemento estructural tipo ladrillo que permite la fijación de elementos eléctricos, ópticos, electrónicos y electromecánicos. Colombia Patent, ref. 14248214.

Veldhuis, A. J. and Reinders, A. H. (2015). Shadow analysis for BIPV and PIPV systems in a virtual environment. *2015 IEEE 42nd Photovoltaic Specialist Conference, PVSC 2015*, pages 1–5.

Viitanen, J. et al. (2015). Energy efficient lighting systems in buildings with integrated photovoltaics.

Vulkan, A., Kloog, I., Dorman, M., and Erell, E. (2018). Modeling the potential for PV installation in residential buildings in dense urban areas. *Energy and Buildings*, 169:97–109.

Wang, D., Cui, H., and Su, G. (2015). A modeling method to enhance the conversion efficiency by optimizing light trapping structure in thin-film solar cells. *Solar Energy*, 120:505–513.

Willoughby, A. A., Omotosho, T. V., and Aizebeokhai, A. P. (2014). A simple resistive load I-V curve tracer for monitoring photovoltaic module characteristics. *IREC 2014 - 5th International Renewable Energy Congress*, pages 1–6.

Willoughby, A. A. and Osinowo, M. O. (2018). Development of an electronic load I-V curve tracer to investigate the impact of Harmattan aerosol loading on PV module pern2tkformance in southwest Nigeria. *Solar Energy*, 166(December 2017):171–180.

XM (2020a). *En Colombia Factor de emisión de CO2 por generación eléctrica del Sistema Interconectado: 164.38 gramos de CO2 por kilovatio hora.*

XM (2020b). *Renovables no convencionales en el SIN.*

Yang, H., Zheng, G., Lou, C., An, D., and Burnett, J. (2004). Grid-connected building-integrated photovoltaics: A Hong Kong case study. *Solar Energy*, 76(1-3):55–59.

Yang, T. and Athienitis, A. K. (2014). A study of design options for a building integrated photovoltaic/thermal (BIPV/T) system with glazed air collector and multiple inlets. *Solar Energy*, 104:82–92.

Yau, H.-T., Lin, C.-J., and Liang, Q.-C. (2013). Pso based pi controller design for a solar charger system. *TheScientificWorldJournal*, 2013:815280.

Yoo, S. H. and Manz, H. (2011). Available remodeling simulation for a BIPV as a shading device. *Solar Energy Materials and Solar Cells*, 95(1):394–397.

Zhang, Y., Stokes, N., Jia, B., Fan, S., and Gu, M. (2014). Towards ultra-thin plasmonic silicon wafer solar cells with minimized efficiency loss. *Scientific reports*, 4:4939.

Zhu, Y. and Xiao, W. (2020). A comprehensive review of topologies for photovoltaic IV curve tracer. *Solar Energy*, 196(May 2019):346–357.